Enhanced damage detection in bridge engineering using DFOS

Julian Unglaub[1*], Aeneas Paul[2], Henrik Becks[3], Zhuo Chen[4], Chongjie Kang[5], Paul Winkler[6], Carsten Könke[6], Thorsten Leusmann[4], Josef Hegger[3], Dirk Lowke[4,7], Martin Classen[3], David Sanio[2], Steffen Marx[5]

[1*]Institute of Steel Structures, Technische Universität Braunschweig, Beethovenstr. 51, Braunschweig, 38106, Germany.
[2]Institute of Concrete Structures, Ruhr University Bochum, Universitätsstr. 150, Bochum, 44801, Germany.
[3]Institute of Structural Concrete, RWTH Aachen University, Mies-van-der-Rohe-Str. 1, Aachen, 52074, Germany.
[4]Institute of Building Materials, Concrete Construction and Fire Safety, Technische Universität Braunschweig, Beethovenstr. 52, Braunschweig, 38106, Germany.
[5]Institute of Concrete Structures, Dresden University of Technology, Street, City, 610101, State, Country.
[6]Institute of Structural Mechanics, Bauhaus-Universität Weimar , Street, City, 610101, State, Country.
[7]Department of Materials Engineering, Technical University of Munich, Freisinger Landstr. 52, Garching / Munich, 85748, Germany.

*Corresponding author(s). E-mail(s): j.unglaub@tu-braunschweig.de;
Contributing authors: aeneas.paul@rub.de; hbecks@imb.rwth-aachen.de; Z.Chen@ibmb.tu-bs.de; chongjie.kang@tu-dresden.de; Paul.Winkler@uni-weimar.de; carsten.koenke@uni-weimar.de; t.leusmann@ibmb.tu-bs.de; jhegger@imb.rwth-aachen.de; lowke@tum.de; mclassen@imb.rwth-aachen.de; david.sanio@rub.de; steffen.marx@tu-dresden.de;

Abstract

Distributed Fiber-Optic Sensing (DFOS) is emerging as a key technology for Structural Health Monitorings (SHMs). DFOS offers strain and temperature measurement over long range with high spatial resolution. This technology is most suitable for large civil infrastructure such as bridges or tunnels Structural Health Monitoring. But early applications were limited to one-dimensional measurements along principal load paths, but recent work has enhanced DFOS with full-field monitoring through fiber-optic grids or with multi-sensor fusion technics.
This paper reviews the state-of-the-art in DFOS-based damage detection for concrete, steel, and steel-composite bridges and highlights new opportunities for enhanced DFOS applications. First, the most common damage characteristics on different bridge types are summarized. A concise collection of published DFOS applications on bridges follows, illustrating integration either surface-bonded or embedded within structural components for short- and long-term monitoring. It is relived that DFOS is routinely used to validate design assumptions, locate crack initiation in concrete members, and monitor crack propagation in steel bridges.
Despite these successes, full-field monitoring with fiber-optic grids remains limited to laboratory scale. Consequently, the paper presents enhanced methodologies for monitoring common damage types: bonding failure, surface cracks, tendon breaks, shear failure, debonding of Carbon Fiber Reinforced Polymer (CFRP) strips, based on embedded DFOS, enhanced 2D fiber-optic grids and multi-sensor fusion. These developments are placed in the context of the Cluster "Damage detection" of the SPP 100+ project "Extending the Lifetime of Complex Engineering Structures through Intelligent Digitalization", which aims to transfer laboratory advances into robust, field-deployable SHM solutions on the Rhine River bridge "Nibelungenbrücke Worms".

Keywords: Bridges, Concrete Structures, Steel Structures, Distributed Fiber-Optic Sensing, Fiber-Optic Grid, Monitoring, Damages

1 Introduction

Distributed Fiber-Optic Sensings (DFOSs) is an emerging technology in the field of Structural Health Monitorings (SHMs), particularly for large-scale civil infrastructure such as bridges and tunnels. Unlike traditional point-based sensors, DFOS enables the high-resolution acquisition of strain and temperature data along the entire length of an optical fiber. Measurement data can almost be collected continuously over distances of up to 100 meters, and with sub-millimeter spatial resolution on shorter sections. The fibers have small diameters and minimal stiffness that allow flexible installation on as-build surfaces or embedding within structures. Additionally, DFOS are intrinsically immune to electromagnetic interference, possesses long-term durability, and, with appropriate coating, can operate reliably in a wide temperature range from $-200°C$ to $800°C$ [1].

A DFOS system typically consists of two main components: the optical interrogator and the distributed fiber optic sensor, which includes the optical fiber itself, its coating, and the adhesive used for bonding to the structure. The sensing principle is based

on one of three scattering phenomena occurring within the optical fiber: Rayleigh, Brillouin, or Raman scattering.

For SHM of bridges, Rayleigh-based sensing is the most commonly used approach due to its high spatial resolution—often in the millimeter range—which makes it particularly well-suited for short-distance measurements up to 100 m length of a fiber. This level of detail enables the detection of localized strain or temperature effects, which are critical for identifying early signs of damage or material degradation [2]. For detailed insights on the different DFOS technics and their theoretical background, it is referred to [1, 3–6].

This paper concentrates on the current state of damage detection based on DFOS on concrete, steel and steel composite bridges and shows the potential of enhanced applications for damage detection based on distributed fiber optics, grids and sensor fusion for bridge engineering. First, typical damages to concrete, steel, and steel composite bridges are described. This is followed by brief collection of applications implemented on bridge structures. In the following, new enhanced methods for detecting common damage types on bridges using DFOS are presented and discussed.

2 Damage types of bridges

Since the 1950s, bridge construction has undergone fundamental changes due to the increased use of modern materials and design principles. Alongside conventional riveted steel truss structures and reinforced concrete bridges, increasingly prestressed concrete bridges and steel bridges with orthotropic decks are being built. This evolution in construction methods has enabled more slender cross-sections and, at the same time, increased span lengths. In retrospect, however, these new structures still have shortcomings in terms of materials, planning, and execution quality, resulting in safety-related challenges that remain to this day. Furthermore, the increase in traffic volume and loads, especially heavy goods vehicles, is accelerating the aging of bridge structures.

Depending on the construction type and design code, the estimated service life of a road bridge is between 75 and 100 years. This indicates that many bridges across Europe, North America and Japan have already reached the end of their service life. But also just 20 year old bridges in China see these challenges, due to the rapid economic growth. However, in order to enable further use, suitable maintenance strategies based on SHM are required. For the implementation of targeted monitoring of damages on bridges, it is necessary to understand the basic types of damage to these bridge structures.

This chapter provides an overview of relevant types of damage to modern prestressed concrete bridges and steel bridges with orthotropic deck slabs from the 1960s onwards. However, many of these types of damage can be applied analogously to other types of concrete and steel bridges as well as steel composite structures. A comprehensive description of bridge construction and its damges can be found in [7–9].

2.1 Damages in concrete bridges

Increasing crack widths or spalling are the most common signs of damage to concrete bridges. Cracks allow chlorides to reach the reinforcement, destroying the passive film and initiating corrosion [10]; corrosion also accelerates when the chloride content exceeds the amount chemically bound in the cement paste. As a consequence degradation of the structure is accelerated and reinforcement or tendon failure can occur [11]. Furthermore, failure without prior announcement is a major problem for concrete bridges. In this context announcement means that large deformations or cracking indicate impending failure. However, this is not always the case for shear cracking or internal tendon breaks with subsequent cross-section failure. These damages are primarily caused by deficiencies in existing concrete bridges, which can be grouped into three categories: Design and material shortcomings, planning and detailing errors and execution-related defects.

Early prestressed bridges often lack of insufficient reinforcement in coupling joints and were designed based on incorrect assumptions (e.g., neglect of temperature-induced stresses [12], creep, shrinkage, and hydration heat). Consequently, the cross-section frequently shifts from the intended uncracked State I to a cracked State II, producing wide cracks that increase cyclic stresses on tendons and raise the risk of fatigue failure. Furthermore, insufficient concrete cover of the reinforcement exacerbates chloride ingress and durability issues. [7]. Corrosion-sensitive prestressing steels used partly until 1990 in Europe, are prone to stress-corrosion cracking, which can cause brittle failure of structures [13]. Many existing bridges do not have today's minimum shear reinforcement, which can result in brittle failure as well, rather from overloading or from cyclic degradation.

Poor concrete compaction, especially in densely reinforced zones, and insufficient grouting of tubes for tendons promote localized corrosion zones. Inaccurate execution and lack of supervision often lead to concrete cover layers that are thinner than specified, increasing the risk of reinforcement corrosion[7].

These interrelated factors, such as design deficits, material vulnerabilities, planning inaccuracies, and execution deficits, drive crack formation, chloride ingress, and corrosion, ultimately reducing the load-carrying capacity and service life of concrete bridges.

2.2 Damages in steel bridges

Orthotropic steel decks have been extensively used in long and medium-span bridges due to many advantages, including high load-bearing capacity, minimal self-weight, efficient erection, and a short construction time. Fatigue damage can be attributed to a combination of factors [14]: increased traffic loads, inadequate fatigue design, poor welding execution quality and significant tolerances during assembly. Furthermore, corrosive influences due to inadequate seal of the roadway lead to the degradation of the steel structures which is amplified by inadequate maintenance. Damage mechanisms in orthotropic bridge decks are categorized into four distinct types based on their location within the load transfer pathway. Category 1, affecting the deck. Subsequent categories address damage to Category 2 (stiffening ribs), Category 3 (crossbeams and

frames), and Category 4 (main girders). Fatigue cracks frequently develop at geometrically complex details, such as welded connections and in transitions with significant stiffness jumps of the components: cracks in the deck plate, cracks in the longitudinal weld between the deck plate and longitudinal trough ribs, cracks in the connection between the longitudinal trough ribs and the transverse diaphragms as well as cracks in the longitudinal splice joints of the main girders [15].

3 Damge detection with DFOS

Several papers and review papers give and overview about the research and applications of DFOS in civil engineering structures [16] [17] [18], [19] [20]. These papers are analyzed based on the application of DFOS on bridges, the damage mechanism and the design of fiber orientation.

According to [17], there exists considerable potential for the utilization of SHM in the domain of maintenance strategies and the predictive maintenance of large infrastructure, such as bridges. The review features mainly results on the measurement of strains to detect spalling or bending cracks based on fibers bonded along reinforcement or on surfaces. One example is given on shear crack detection on concrete surfaces based on a two-dimensional DFOS grid [21]. The role of the coating system in facilitating permanent bonding and ensuring reliable results has been identified as a significant aspect of the field. Achieving this standardized application process is crucial. However, this review mainly features studies on one-dimensional application of DFOS.

Bado and Casas [18] provide a comprehensive overview of research on SHM using DFOS. It highlights the main advantages of DFOS, such as minimal intrusiveness, high accuracy, and high spatial resolution in strain, temperature, and vibration monitoring. Deployment strategies and applications across a wide range of cases are presented comprehensively, including laboratory experiments, bridges, buildings, geotechnical structures, tunnels, pipelines, and wind turbines. The focus is on measuring strains using DFOS bonded to reinforcement in concrete structures or bonded to concrete surfaces to detect cracks. The review underlines a strong emphasis of DFOS on measuring along the primary load-bearing direction of the component. The first applications of fiber grids to enable two-dimensional measurements on the component surface are also becoming apparent. However, there is no critical evaluation and discussion of the outcome of the individual study.

Gowshikan et al. [19] selectively review studies and applications of DFOS in civil engineering such as bridge, tunneling and railway monitoring. No metric is given for the selection of the work presented nor for the conclusions. It is generally concluded that there is great potential for the construction industry and that the measurement techniques provide reliable results. For bridges, the main damage mechanism of interest is cracks in concrete and strains during loading tests of structures based on one-dimensional sensor orientation.

Howiacki et al. [20] show the growing use of DFOS in concrete, steel, and composite bridges in Poland, highlighting both local and large-scale monitoring with a focus on data analysis along the fiber. While DFOS proves effective, especially with embedded sensors, research gaps remain regarding long-term adhesive installations, standardized

data evaluation, and user-friendly automated systems. Broader adoption is limited by high costs, insufficient experience, and lack of standardization. The review mostly focuses on embedded sensors in concrete, but it also highlights the local application of DFOS to track crack propagation on welds. However, all examples are limited to 1D applications of fibers.

It shows that the small form factor and flexibility of optical fibers allow for their seamless integration into bridge structures—either bonded to the surface or embedded within components such as decks, girders, or support structures. This enables short or long-term, non-intrusive monitoring of strain and temperature distributions across large areas. By capturing spatially continuous data, DFOS provides early indications of damage or degradation, such as crack formation, bonding failure or tendon breaks. Mentioned applications are mostly related to reinforced concrete structures. Only few applications are on steel structures, mostly monitoring spanned cables or main girders. In general the focus has been on monitoring along a main grinders along the structure of interest. More recent research has extended the scope for the application to full-field measurements via fiber grids. However, fiber grids or sensor fusion of fibers with other sensors like strain gauges, Digital Image Correlation (DIC) or acoustic emission is still related to laboratory scale.

4 Application of DFOS in Bridge Monitoring

This section investigates the application of DFOS technology in bridges, emphasizing its role in detecting and monitoring damage. Through a comprehensive review of case studies, the current state of application of DFOS to detect damages on bridges is demonstrated, see Table 1 and Table 2. It provides an overview of bridges equipped with DFOS-based measurement systems based on published cases. The tables also lists the length L of the DFOS sensors utilized, which varies between 4.0 and 1000 m. Most cases use Rayleigh back scatter, and the latter one Brillouin. Data not mentioned in the literature is indicated with a '-'.

4.1 Concrete Bridges

In the case of concrete bridges, a distinction can initially be made by the sensor installation. In new constructions, DFOS is usually embedded in the concrete (e.g. *Streicker Bridge*, *Nine Wells Bridge*) to monitor the strain or temperature distribution. Alternatively, the sensors can also be attached to the reinforcement (*Musmeci Bridge*, *Reinforced Concrete Bridges*). In this case, peaks in the strain signal are used to locate concrete cracks.

For use in existing structures, DFOS is applied to the concrete surface. They are also used here to localize concrete cracks. In addition to monitoring during regular operation (*Redzinksi Bridge*) or at sensitive points such as the coupling joint (*Highway Bridge*), DFOS was also used to monitor the formation of cracks induced by tendon breaks (*Kreuzhof Bridges*) or an extension of the bridge (*Sarajevo Bridge*).

In addition to crack monitoring, the focus of DFOS systems is on determining the strain distribution. In this context, DFOS were used in milled grooves (*Bridge A6358*, *Bridge #1330005*, *Bridge on Walter St.*) or bonded to the concrete surface

(*Black River Bridge*) in static load tests. An alternative method for the subsequent application of DFOS was tested on the *Grist Mill Bridge* and used to evaluate the strain distribution. Here, DFOS were embedded in a textile, which was subsequently applied to the bridge. Further applications of DFOS were realized on concrete bridges, namely for the quantification of the stress losses on a railway bridge in Great Britain and for the safety assessment of a railway bridge in Taiwan after an earthquake.

No.	**Name**	**Location**	L **[m]**	**Year**	**Monitoring Objective and Target Component**	**Source**
1	Sarajevo Bridge	Spain	50.0	2015	Strain distribution and cracking along a main girder during construction	[22]
2	Railway Bridge	Great Britain	≈ 25.0	2015	Strain and temperature distribution for pre-stress loss quantification	[23]
3	Streicker Bridge	United States	≈ 40.0	2010	Embedded DFOS in concrete as an on-side laboratory	[24]
4	Bridge #1330005	United States	$2 \cdot 7.93$	2006	Strain distribution in a static load test	[25]
5	Bridge on Walters St.	United States	$2 \cdot 6.58$	2006	Strain Distribution in a static load test	[25]
6	Bridge A6358	United States	$2 \cdot 56.0$	2006	Strain Distribution in a static load test	[25]
7	Black River Bridge	Canada	≈ 30.0	2013	Strain distribution during a load test to investigate the performance of DFOS	[26]
8	Musmeci Bridge	Italy	80.0	2021	Measurement of strain, displacement and temperature by DFOS integrated in Glass Fiber Reinforced Polymer (GFRP) bars	[27]
9	Reinforced Concrete Bridge	Germany	8.0	2023	Crack monitoring by monolithic sensors tied to the reinforcement	[28]
10	Reinforced Concrete Bridge	Germany	4.0	2023	Crack monitoring by monolithic sensors tied to the reinforcement	[28]
11	Kreuzhof BW 40/45 and BW 40/46	Germany	< 100.0	2021	Strain distribution due to static mechanical loading and temperature changes	[29] [30]
12	Highway Bridge	Germany	$4 \cdot 25.0$	2021	Strain distribution and development of cracks at the coupling joint	[31]
13	Nine Wells Bridge	Great Britain	$6 \cdot 3 \cdot 50.0$	2008	Strain and temperature distribution by sensors embedded in concrete	[32]
14	Railway Bridge	Taiwan	$\approx$1000.0	2024	Deformation from static loadings to ensure safety after earthquakes (Brillouin)	[33]
15	Grist Mill Bridge	United States	$2 \cdot 21.0$	2023	Strain Distribution with a modified installation method	[34]
16	Redzinski Bridge	Poland	$\approx 4 \cdot 30.0$	2020	Development of crack widths	[35]

Table 1: Published applications of DFOS on concrete bridges.

4.2 Steel / Steel-Composite Bridges

DFOS as a tool for steel bridge damage monitoring allows diffrent applications clustered around specific damage causes and detection methods. A primary focus is fatigue crack detection, addressing damage from cyclic loading. For example, in the *Götaälvbron Bridge* and *Normandie Bridge*, DFOS helps to identify new fatigue cracks and stress concentrations in welds and orthotropic decks. These applications showcasing its ability to detect early damage and monitor crack propagation.

Another application involves long-term performance and aging of structures, where DFOS evaluates loading history, fatigue and environmental effects. In the *Haicang Bridge*, DFOS monitored strain distribution in steel box girders, providing insights into structural health after years of service. Similarly, in the *Baluarte Bridge*, DFOS was used to study vibration-induced fatigue in the steel girders.

For damage due to overloading or increased traffic loads, DFOS was used in the *John Counter Boulevard Bridge* and *Old Steel Railway Bridge Operated* to detect deformation, and potential failure in truss members and steel beams.

DFOS aids to validated design assumptions, as seen in the *Baluarte Bridge* and *Carrizo Bridge*, where unexpected strains in lower flanges and near pylons were discovered. In the *University Bridge in Bydgoszcz*, DFOS revealed stress concentrations in the cable anchorages caused by structural deficiencies. By monitoring these regions, DFOS provided critical insights into the structural behavior during strengthening.

4.3 Clustering of DFOS application on bridges

Given the scope and complexity of employing DFOS technology for damage-centric bridge monitoring, a systematic classification approach has been adopted: The classification is based on the types and objectives of monitoring:

- **stress and structural integrity monitoring**: The focus is on the application of DFOS techniques for monitoring the strain distribution, deformation state, and structural integrity of bridge structures, with a particular emphasis on detailed analyses of crack development (concrete), the effects of prestressing and areas of stress concentration (fatigue).
- **dynamic behavior and vibration monitoring**: The implementation of DFOS technology for capturing the vibrations and behavior of bridges under dynamic or cyclic loads (e.g., traffic load history, wind induced effects) has been investigated.
- **temperature and environmental effect monitoring**: The utilization of DFOS technology for monitoring temperature variations and their impact on bridge performance has been explored.

The clustering of the applications of DFOS on bridges shows a similar result to the analysis of the literature, section 3. Main benefits are seamless integration into bridge structures—either bonded to the surface or embedded within components. Both short or long-term monitoring of strain or temperature distributions across large areas are possible. A common application of DFOS in steel and concrete bridges is the validation of design assumptions. DFOS is used in monitoring to detect cracks origin from various damage types, particularly in concrete bridges. In steel bridges, crack monitoring is

No.	Name	Location	L [m]	Year	Monitoring Objective and Target Component	Source
1	Brama Przemyska Bridge in Przemyśl	Poland	33	2017	local strain distribution of lower flange	[20]
2	T. Mazowiecki Bridge in Rzeszów	Poland	600	2018	displacement and deformation profiles of the steel girder	[20]
3	University Bridge in Bydgoszcz	Poland	18	2021	strain distributions in steel cable anchorages	[20]
4	A Bridge in Warsaw	Poland	80	2021	-	[20]
5	New Steel Arch Truss Bridge in Kraków	Poland	8	2022	strain distribution of a steel toothed anchor	[20]
6	Highway Bridge in the Austrian Alps	Austria	160	-	vibration, deformation and strain of steel-concrete composite sections	[36]
7	Götaälvbron Bridge	Sweden	270	2007	fatigue cracks, strain of critical steel girders	[37]
8	Normandy Bridge	France	-	-	fatigue damage in the orthotropic steel deck, specifically welded joints	[38]
9	Terraglio Est Bridge in Padua	Italy	-	2016	strain distribution of Continuous Fly Auger pile in the foundation raft	[39]
10	John Counter Boulevard Bridge	Canada	15.5	2020	support reactions and detect damage in steel beams	[40]
11	Newmarket Bridge	Canada	4	2020	strains in rails of the bridge superstructure	[41]
12	Mile 17.7 Grimsby Subdivision CN Railway Bridge	Canada	20	-	strain in steel truss members and connections	[42]
13	No. A6358 Bridge	USA	-	-	strain distribution and deflection profiles of the steel girders	[43]
14	Baluarte Bridge	Mexico	-	-	strain distributions of the lower flanges	[44]
15	Carrizo Bridge	Mexico	-	-	strain distributions, vibrations of the lower flanges	[44]
16	Haicang Bridge	China	1084	2015	strain and temperature variations along the bottom girder	[45]
17	Old Steel Railway Bridge Operated	Malaysia	31.4	2017	strain distributions of the bottom chord of the steel truss	[46]

Table 2: Published applications of DFOS on steel bridges.

performed indirectly via the redistribution of strains close to (possible) damage areas. It has been found that DFOS is used alongside other sensors, such as strain gauges, accelerometers and acoustic emission sensors, in bridge applications. These systems are operated and evaluated individually. Data is only combined manually if necessary. In general, the focus has been on monitoring along a main structure or on preselected local damaged zones. Full-field measurements via fiber grids is currently not present in application.

5 Enhanced damage detection with DFOS

As the previous sections showed there is a need for research on fiber grids or sensor fusion of fibers with other sensors like stain gauges, DIC or acoustic emission to enhance damage detection on bridges. The following section presents improved methods for damage detection on bridges that use DFOS as the central measurement technology. For each method presented, the type of damage addressed, measurement configuration, and exemplary results are briefly presented and discussed.

5.1 Monitoring of bonding failure

5.1.1 Characteristics of the bond behaviors

The long-term safety and serviceability of concrete bridges depend critically on the integrity of the bond between reinforcement and the surrounding concrete, as this bond ensures the effective force transfer and crack control. Inadequate bond behavior can compromise load distribution, lead to excessive cracking, and ultimately reduce the durability and reliability of bridge structures. Bond degradation may result from varoius damge mechanisms: e. g. corrosion-induced expansion, (cyclic) loading, temperature gradients, or inadequate construction execution. Traditional inspection techniques such as visual surveys, spot strain gauges, or ultrasonic testing, provide only information on the surface and fail to capture internal bond deterioration. Despite its many advantages of conventional steel rebars, the corrosion of steel in salty or extreme environments remains a crucial challenge. As an alternative, GFRP rebars offer high corrosion resistance and lower maintenance requirements. To monitor the bond behavior of GFRP rebars, integrating embedded DFOS can enable continuous observation of the bond state and allow the detection of debonding at an early stage, before macroscopic cracking occurs [47].

5.1.2 Measuring concept and damage detection

Figure 1 schematically shows the principle of the bond specimen with one GFRP bar. Each bar is 1280 mm long and was embedded in concrete with a bond length of 300 mm. The distributed fiber optical sensors (DFOSs) were installed in the bar grooves to measure the bond strains along the embedded bars in bond specimens. For each GFRP bar, an anchorage steel tube of 380 mm in length was used at the loaded end. The concrete specimen had an external dimension of 400 mm x 200 mm x 200 mm To prevent splitting failure of the concrete, four 300 mm longitudinal reinforcement steel bars (d = 8 mm) and six steel stirrups ($d = 8$ mm) at a distance of 50 mm were applied. The tests were conducted with a displacement-controlled loading rate of 0.5 mm/min.

Current researches show various results and conclusions when different types of DFOSs or adhesives were applied. Moreover, these studies are primarily limited in the area of steel-reinforced components and carbon composites and lack comprehensive investigations. Considering the two most commonly used DFOSs, namely polyimide (PO) and acrylate (AC) coatings, along with the adhesives epoxy (EP) and cyanoacrylate/silicon (CN/SI), four DFOS and adhesive combinations are generated in bond tests. In addition, each combination has two specimens.

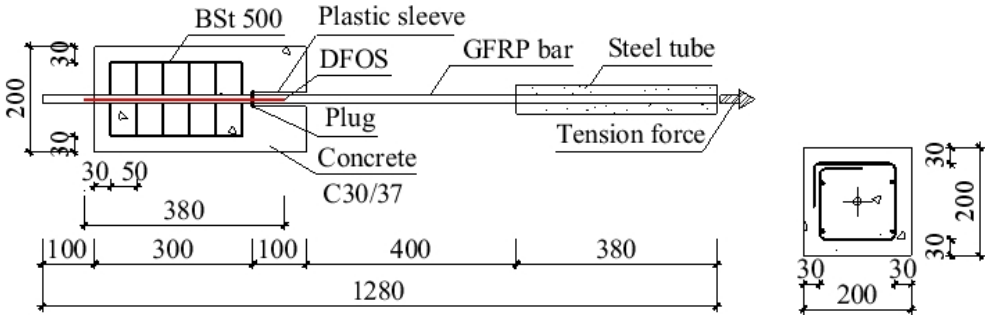

Fig. 1: Bond test schematic: overview (left) and cross-section (right) [47]

In order to avoid DFOS rupture in concrete, each DFOS was installed in a groove that was pre-cut by a machine Figure 2. Afterwards, adhesive was filled into the groove Figure 2. It is also essential to ensure good adhesive quality.

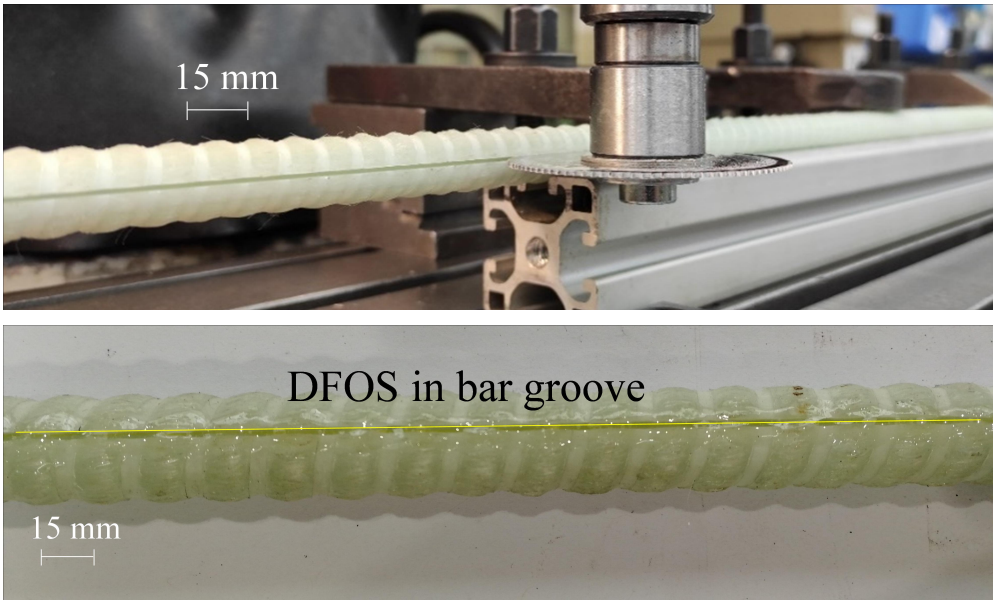

Fig. 2: DFOS application on GFRP bars [47]

5.1.3 Results

Figure 3 displays the strain distributions of the four combinations under different tensile loads. The strains of the bars outside of the concrete are also calculated based on the assumption of elastic modulus $E = 47\,\text{GPa}$. Hence, a theoretical value can be calculated: $\epsilon = \frac{F}{E \cdot A}$, where F is the load and A is the cross-sectional area.

It can be observed that the strains increase from the free end to the loaded end gradually in a non-linear manner. Strain differences occur and become more evident when the load increases.

In general, the specimens with polyimide DFOSs measure larger strains than the acrylate DFOSs. Besides, the polyimide DFOSs measure constant strain distributions of the bars outside of the specimens. This corresponds to the real condition that the bar is under a constant normal force. In contrast, the acrylate DFOSs measure decreased strain distributions outside the concrete. These differences can be attributed to the stiffer coating of polyimide sensors, which facilitates robust and accurate strain transfer. However, this also leads to earlier sensor failure. For instance, the polyimide DFOSs were damaged at up to 11 000 µϵ, whereas the acrylate DFOSs failed at up to 15 000 µϵ.

In conclusion, polyimide coating DFOSs can be applied where measuring the detailed local strains due to the features of high strain sensitivity. In comparison, acrylate DFOSs can be applied on long and curved specimens with the features of flexibility and the changeable strain introduction lengths.

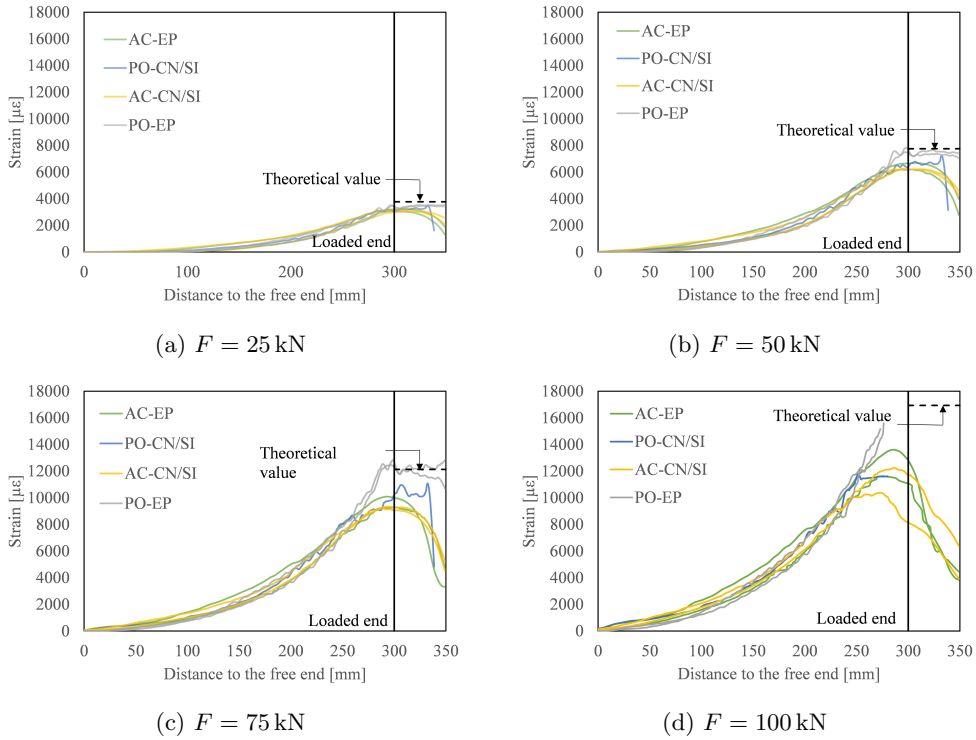

(a) $F = 25\,\mathrm{kN}$ (b) $F = 50\,\mathrm{kN}$

(c) $F = 75\,\mathrm{kN}$ (d) $F = 100\,\mathrm{kN}$

Fig. 3: Comparison of the measured strains using various combinations of DFOS and adhesives. [47]

As a result, it can be concluded that DFOSs are capable of accurately and robustly capturing the full bonding strain distribution of embedded GFRP bars in concrete with proper configuration and installation.

5.2 Monitoring of surface cracks with internal sensors

5.2.1 Characteristics cracks in concrete

Embedding DFOS in concrete enables continuous monitoring of internal strain, capturing crack initiation and propagation that surface sensors often miss. In this caase, DFOS enables full-length strain measurements within the concrete, detecting subtle changes before visible cracking occurs. Protected from environmental damage, embedded DFOS also offer high-resolution, long-term insight into strain redistribution, crack evolution, and structural behavior, making them a effective tool for durability assessment and SHM [48].

5.2.2 Measuring concept and damage detection

Figure 4 illustrates the setup for the four-point flexural tests conducted on specimens measuring 200 mm x 550 mm x 3700 mm with lap-spliced a hybrid connection of GFRP bars and stainless-steel bars (S-Steel). Figure 4 shows the detailed reinforcement configuration of the specimens. Seven GFRP bars and seven S-Steel bars were constructed on both sides. They overlapped in the middle of the span with a specified lap-spliced length (300 mm). Due to the limited investigations on the concrete crack in hybrid lap-spliced specimens, Epsilon DFOSs Figure 5 were positioned at the same height as the lap-spliced bars to monitor the concrete strain and crack developments.

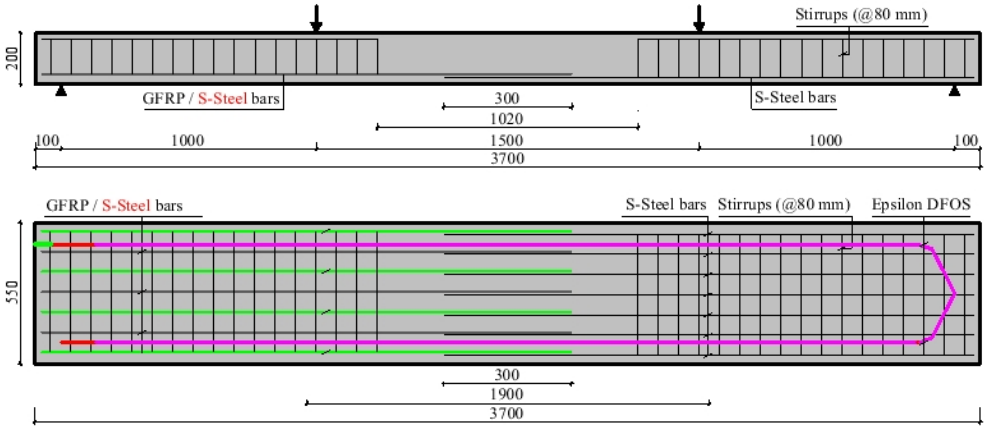

Fig. 4: Bar and DFOS arrangements: side view (top) and top view (bottom= (dimensions in mm) [49]

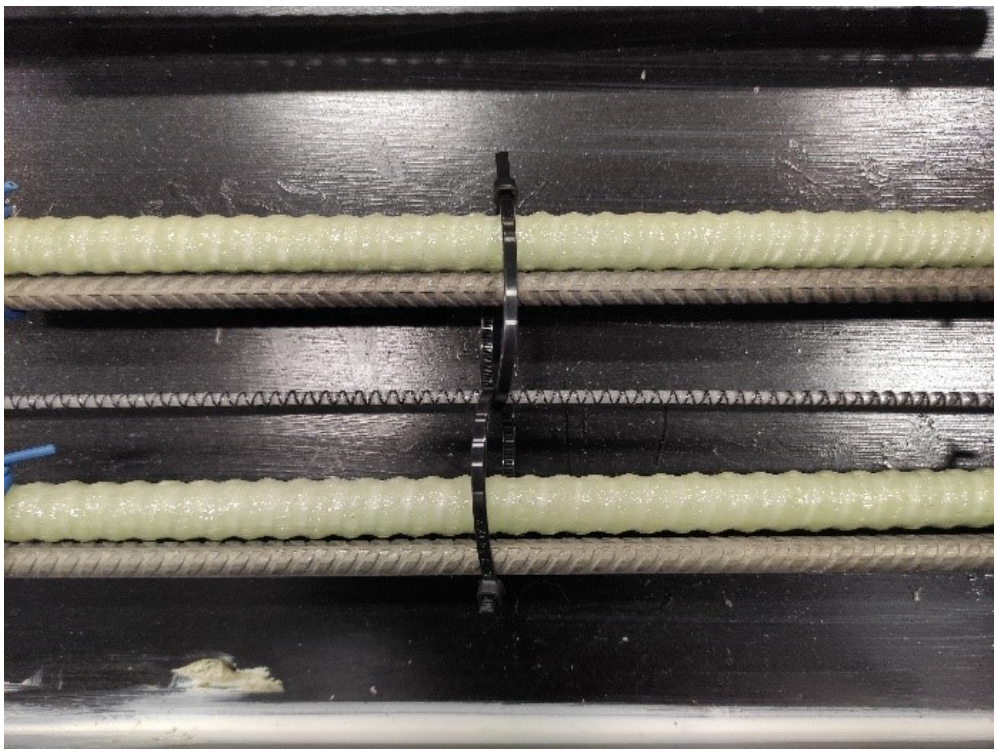

Fig. 5: Photograph: Bar and DFOS arrangements top view [49]

5.2.3 Results

Figure 6 shows the marked concrete cracks (using a pencil) observed with naked eyes and the concrete strain distribution obtained from the Epsilon DFOS at the middle-span displacement of 40 mm. It can be seen that there is a good agreement in the crack location between the marked and Epsilon DFOS measurements. In total, visual inspection identified 4 cracks in the lap-spliced area, 11 cracks on the GFRP bar side, and 10 cracks on the stainless steel bar side. In comparison, the Epsilon DFOS detected 4, 15 and 16 cracks in the respective areas. This difference can be attributed primarily to the ability of the Epsilon DFOS to detect smaller cracks (numbered 1-3 and 32-35) that were difficult to observe with naked eyes.

The concrete crack width is calculated by integrating the concrete strain profile over a certain length adjacent to the crack and eliminating the contribution of the tension stiffening between cracks. It has been repeatedly proven that this method agrees well with DIC technology. The equation is as follows:

$$w_{crit,i} = \int_{l^-_{t,i}}^{l^+_{t,i}} \epsilon^{DFOS}(x)dx - \rho\alpha \left[\int_{l^-_{t,i}}^{l^+_{t,i}} \hat{\epsilon}(x) - \epsilon^{DFOS}(x)dx \right] \tag{1}$$

Where ϵ^{DFOS} is the measured strain along the Epsilon DFOS coordinate $x, x_{cr,i}$, ϵ is the assumed linear strain variation between cracks neglecting the steel-concrete interaction, $\rho = \frac{A_s}{A_{c,ef}}$ and $\alpha = \frac{E_s}{E_c}$ are the reinforcement ratio and modular ratio, respectively and $l^-_{t,i}$ and $l^+_{t,i}$ are the transmission lengths to the left and right sides of the i^{th} crack $w_{cr,i}$.

It is evident that the crack widths are most pronounced at the two lap-spliced ends, owing to the discontinuity of the overlapping bars. Conversely, the crack widths are minimal in the middle lap-spliced region due to the presence of double-reinforced bars. Furthermore, the crack widths remain consistent in the pure bending areas, and decrease in the bending-shear area, which aligns with the actual behavior observed in concrete specimens subjected to four-point flexural loading.

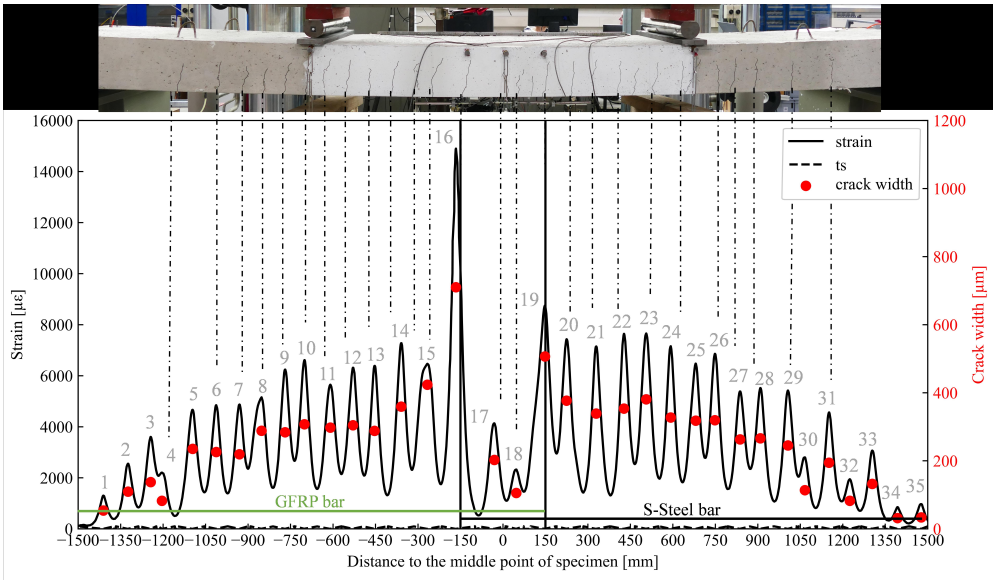

Fig. 6: Comparison of crack distribution between specimen surface and Epsilon DFOS data in GS-300(1)

At the same time, the results are compared with DIC in Figure 7, of which the measurement range is limited to the center 100 mm length of the specimens. Figure 8 shows the calculated crack based on methods. In general, DFOS and DIC show very good consistency with minor discrepancies.

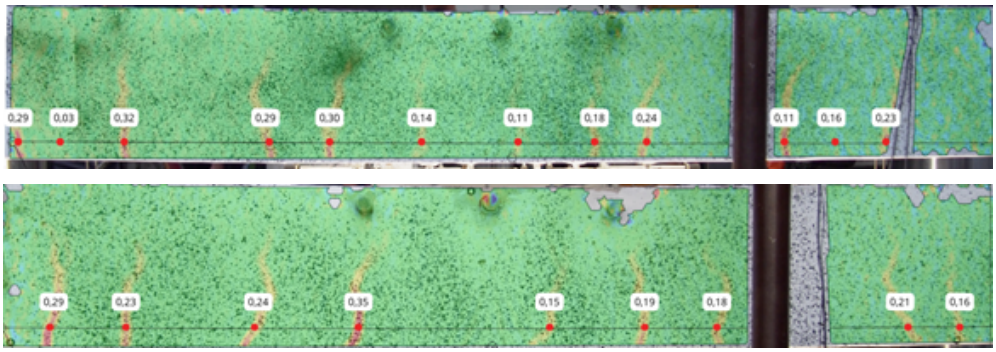

Fig. 7: DIC crack patterns from BK1 (top) and BK2 (bottom), L-300 beams

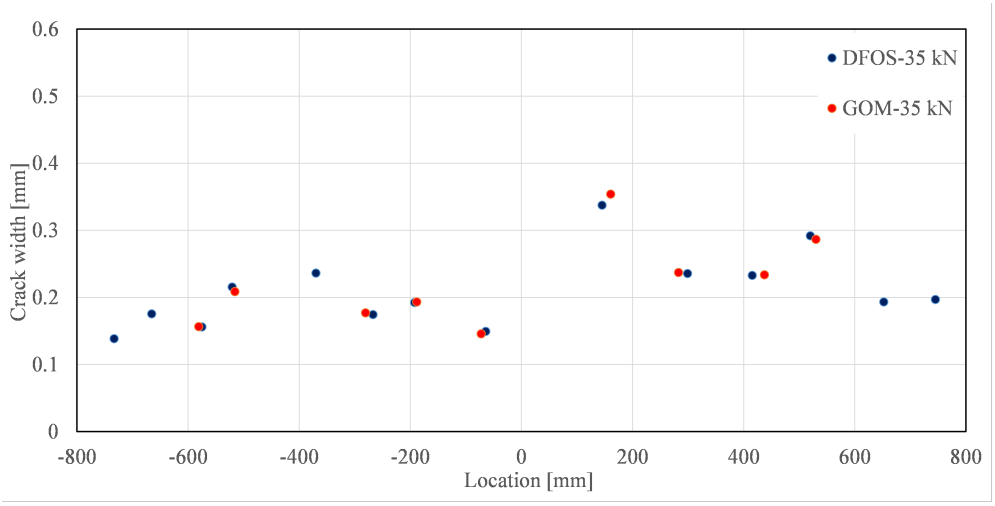

Fig. 8: Crack measurements of the beams at 35 kN

5.3 Monitoring of Internal Tendon Breaks using DFOS

5.3.1 Characteristics of the damage mechanism tendon break

On prestressed concrete structures, DFOS broaden the spectrum to localize and quantify internal tendon breaks [50, 51]. Such damage is caused, for example, by fatigue [52] or stress corrosion cracking [53] and is usually not visually recognizable from the outside. It leads to localized loss of stress, both in the tendon (σ_p) and in the concrete (σ_c). Due to re-anchoring in the surrounding grout and concrete, the lost prestress is rebuilt over an anchorage length l_bp. Depending on the bond conditions and tendon type, anchorage lengths in the range of a few decimeters [54] to meters [55] are common. In addition to the deformation along the tendon with relative displacements between tendon and grout and associated bond stresses τ_b, a wedge effect of the tendon (so-called HOYER effect Briere et al. [56]) occurs at the point of break due to elastic reforming of the tendon's cross-section tapered by the prestressing. The mechanical behavior of the prestressing steel in the case of a tendon break is shown in Figure 9. The locally introduced anchorage forces propagate from the breakpoint to the concrete surface, where they can be recorded and localized as a change in strain using DFOS.

5.3.2 Measuring concept and damage detection

For certain cases of damage (e.g. coupling joints for fatigue-induced breaks [57]), the sensitive positions for tendon failure are known in advance. However, tendon failures may occur along the entire structure. A two-dimensional grid of DFOS along the tendon cable enables global monitoring of the structure and can be installed on both new and existing buildings. The sensors are applied with several fibers parallel to the tendon axes. The use of an additional second orthogonal fiber direction increases the robustness of the measuring system (e.g. against bending cracks [58]) and provides redundancy. Such an application, orientated on a parabolic tendon profile, is sketched in Figure 9.

The changes in the strain field caused by tendon breaks are small, especially at great embedment depths. With high-precision measuring systems, however, detection is still possible down to depths of 40 to 50 cm [59]. Thus, a measurement configuration with the highest possible accuracy is recommended. With common systems (e.g. Luna ODISi 6108), an accuracy of $\pm 2\,\mu\mathrm{m/m}$ is possible with a gauge length of 2.6 mm. The combination of a two-component adhesive (Polytec AC2411; based on epoxy resin) and a fiber with a comparatively rigid polyimide coating ($E_\mathrm{Polyimide} = 400 \cdot E_\mathrm{Acrylate}$) ensures the transmission of low strain changes [60]. Although this configuration is prone to fracture and potential sensor failure at steep strain gradients [61, 62], this is not an issue at low strain changes ($\leq 200\,\mu\mathrm{m/m}$) without cracking as characteristic of the damage case at hand. Once installed on the concrete surface (cf. [63]) each gauge is associated an unique position (x, z). Bi-linear interpolation Paul et al. [58] is used to approximate the strain field by sets of four gauges arranged square (cf. Figure 10).

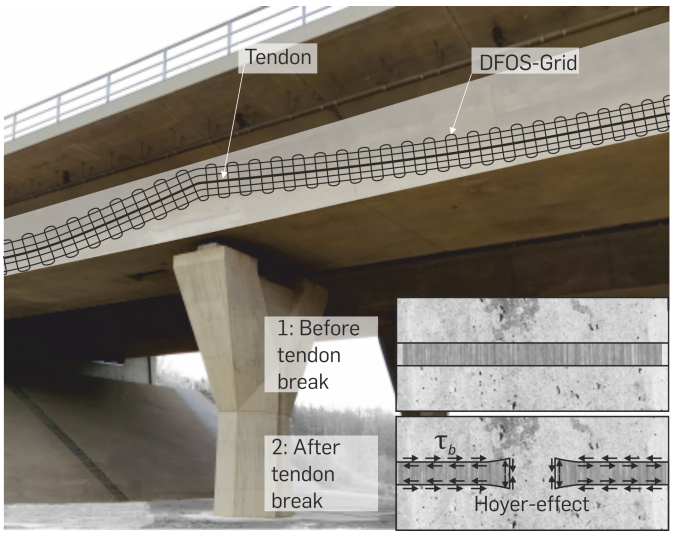

Fig. 9: Conceptual layout of a 2D measuring grid made from DFOS to detect broken tendons orientated towards the tendon profile and induced mechanical stresses (D. Sanio, A. Paul)

5.3.3 Evaluation and results

The measurement system was validated in experimental tests (for details see [54, 58, 59]). Artificial tendon breaks were generated on prestressed members while the resulting strain changes were recorded on the concrete surface using a two-dimensional measuring grid. The distance between the parallel sensor strands varied between 4 to 7.5 cm using the configuration described above. The results refer to a reference time t_0, which corresponds to the prestressed condition in the experiments.

Characteristic strain fields for tendon breaks were identified in the investigations. Figure 10 visualizes the measured strain fields due to tendon failure in longitudinal (a,b; $\Delta\varepsilon_{c,x}$) and transverse (c; $\Delta\varepsilon_{c,z}$) directions of two tests. In direction of the tendon, low tensile strains relative to the prestressed state occur locally at the breakpoint, followed by a maximum of tensile strains at anchorage. From there, the strain field decreases steadily until the full prestress is reintroduced into the member. Perpendicular to the tendon axis, the longitudinal strain changes also decrease, to the bottom superimposed by bending effects induced by the test setup. The analyses show that the propagation of the strain field significantly depends on the embedment depth [59] and the bond properties [54]. High bond stiffness reduces the development and propagation of the strain field in longitudinal direction, see Figure 10b. In all tests a detection with strain fields clearly above the measurement noise is possible.

Perpendicular to the tendon axis, ellipsoidal compressive strains occur locally at the point of break. By value, these are significantly smaller than the corresponding strains in direction of the tendon (approx. factor 5; see Figure 10c). And they lower much faster than the longitudinal strains with increasing distance from the breakpoint and in the test become zero in about 6 cm (in both the x and z directions). At a greater

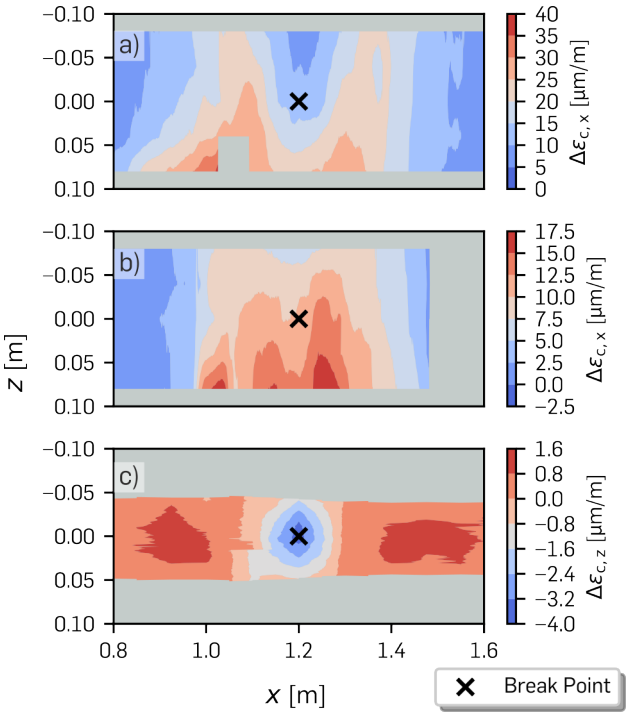

Fig. 10: a) strain changes along the tendon ($\Delta\varepsilon_{c,x}$) in normal strength concrete at $\Delta y = 0.15\,\mathrm{m}$ b) the same for high strength concrete, and c) perpendicular to the tendon axis ($\Delta\varepsilon_{c,z}$) in normal strength concrete (A. Paul)

distance (∼25 cm) from the point of break, small tensile strains occur in transverse direction (∼2 µm/m) due to the introduction of longitudinal prestress. Overall, the transverse strain field is much less pronounced. Clear detection is only possible for shallow embedment depths of up to ∼25 cm. Interference might overlay the break-induced strain field and impedes detection. In the case of concrete cracks (e.g. from bending) that cross the longitudinal fibers, local strain peaks (up to ∼2000 µm/m); Figure 11c) are induced into the strain field in longitudinal direction. Then, strains due to tendon breaks are virtually no longer recognizable. However, detection is still possible using the transverse strains (Figure 11d). Similarly, the transverse direction can also be used to identify temperature-induced disturbances [64]. Local heating, which was simulated in the experiments with a heating mat ($\Delta T = 40\,\mathrm{K}$ [65]), can cause strain fields like those of broken tendons in direction of the tendon, as shown in Figure 11a. However, in the transverse direction (Figure 11b), unlike tendon failure, it leads to strains in the same range of values as in longitudinal direction (see Fig. 11b). Despite external interferences, the combined evaluation of the characteristic strain fields in the longitudinal and transverse directions enables to reliably detect tendon breaks. DFOS surface grids extend the portfolio of methods to detect internal tendon breaks and are particularly suitable for permanent monitoring of existing structures.

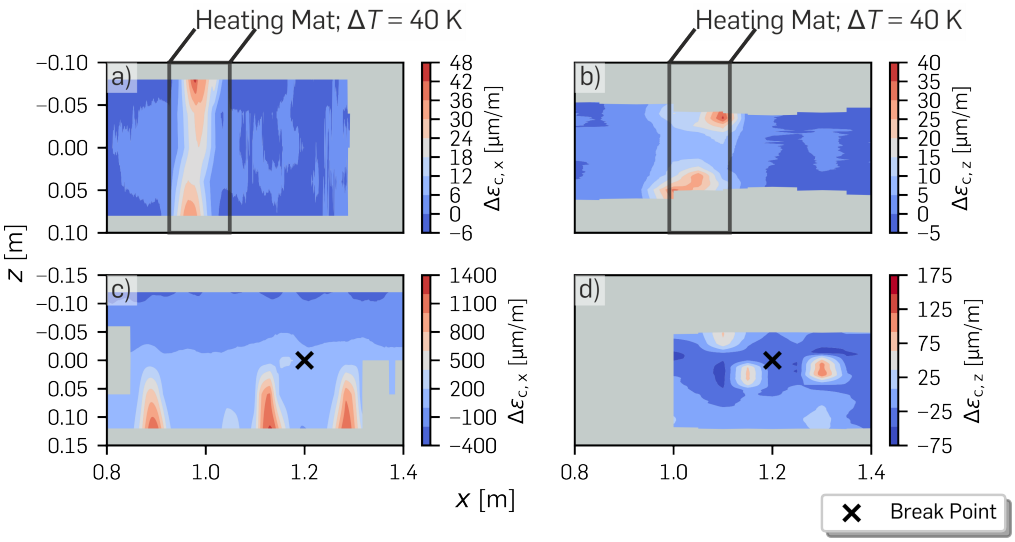

Fig. 11: Impact of interference on the longitudinal strain field: strain fields induced by local temperature change along (a) and across (b) the tendon, strain fields induced by a broken tendon combined with load induced cracking along (c) and across (d) the profile (A. Paul)

Based on the test results, it seems possible to detect tendon breaks down to embedment depths of 45 to 50 cm. The true limits of the method are currently investigated in ongoing experimental campaigns and an application of the fiber grid on the Rhine River bridge "Nibelungenbrücke Worms" is planed.

5.4 Monitoring shear failure of RC structures using 2D-FOS

5.4.1 Characteristics of shear failure

More than 85% of all bridge structures on German federal highways (in terms of surface area) consist of prestressed or reinforced concrete [66]. Particularly in the case of older prestressed concrete bridges constructed according to outdated design concepts with minimal reinforcement, recalculations based on current engineering standards [67, 68] frequently reveal significant structural deficits [69]. One particularly critical failure mechanism is observed in the web region, where combined shear and torsional stresses can lead to diagonal cracking. These cracks may ultimately result in either tensile failure of the shear reinforcement or a strut-and-tie failure mechanism. While experimental studies have demonstrated that repeated loading can be sustained for thousands of load cycles even after macro-crack formation [70], conventional localized measurement techniques are inadequate for effectively monitoring the onset and propagation of cracks. For an accurate assessment of shear crack formation and progression, a two-dimensional resolution is essential. To address this challenge, the measurement concept *2D-FOS* was developed [71], enabling two-dimensional strain and crack width measurements through an externally applied fiber optic sensor network. The application concept of 2D-FOS has been designed to allow for both high-resolution strain measurement prior to crack formation and long-term monitoring after crack formation. To analyze the raw data, an algorithm was developed to automatically compute strain profiles, crack positions, and crack widths in 2D.

5.4.2 Measurement prior to macro-crack formation

To systematically evaluate the 2D-FOS application concept, an extensive experimental campaign was conducted, including various uniaxial tensile tests on reinforced and plain RC specimens (100 cm x 12 cm x 4.5 cm) [72, 73]. The primary focus of these investigations was on measurement accuracy, reliability, sensor orientation, crack localization, and crack width computation. Given that all bridge structures are subjected to repeated loading – particularly from traffic – the influence of cyclic loading was also examined. Figure 12a-c presents strain measurement results from a notched plain concrete specimen subjected to monotonically increasing loading until macro-crack formation. Each macro-crack initiates with the successive development of micro-cracks within the concrete matrix. Initially, this micro-crack development manifests as an increase in the area-specific mean strain level, eventually leading to localized strain concentrations. While the mean strain starts out very low, it gradually increases throughout the experiment. As the test progresses, strain begins to concentrate at the specimen's center, between the two notches (Figure 12b). Just before failure, the strain concentration intensifies noticeably on one side, highlighting the propagation of the macro-crack across the specimen (Figure 12c). The mean fracture strain ultimately reaches approximately 100 microstrain (0.01%), closely aligning with typical fracture strain values for concrete (e.g., [74]). Notches facilitate micro-crack development in a localized region, prompting an earlier onset of strain concentration. In the

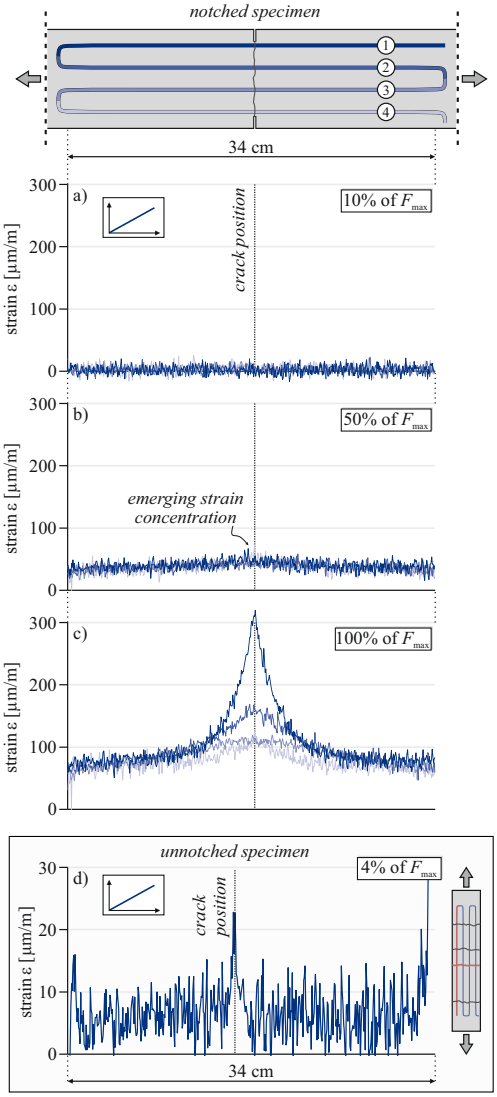

Fig. 12: a-c) Cracking process of a monotonically loaded notched specimen without reinforcement and d) crack localization detected in an monotonically loaded reinforced specimen.

absence of notches, significant strain concentration often occurs later. However, various tests within the study have shown that even minor defects in the concrete matrix act as "natural notches," initiating micro-crack growth at an early stage (Figure 12d).

Nevertheless, for the earliest and most reliable crack detection (prior to macro-crack formation), analyzing the area-specific mean strain remains the most effective approach. This methodology is particularly beneficial under fatigue loading, as it

enables crack propagation detection even in the absence of clearly visible strain concentrations, thereby facilitating an approximation of crack initiation. Figure 13 illustrates the displacement development of δ_{FOS} for a fatigue-loaded specimen. Here, δ_{FOS} represents the micro-crack opening displacement, computed by integrating all strain measurements within a fiber segment over its entire length (34 cm). For better visualization, only the displacement at maximum load (S_{max}) is depicted for each load cycle.

The mean displacement of all fiber segments is shown in dark blue, illustrating the characteristic three-phase displacement progression observed in fatigue testing. The comparison between the displacement at the phase transition from Stage II to Stage III (Figure 13a) and the fracture displacement from a monotonically loaded specimen (Figure 13b) reveals a strong correlation (small $\Delta\delta$), supporting the hypothesis of a threshold relationship, as previously suggested by [75]. However, the scatter band of measured strains, highlighted in light blue, also illustrates that even minor deviations in displacement $\Delta\delta$ can lead to substantial variations in the predicted remaining load duration Δt. A more detailed analysis of the discussed experiments can be found in [73].

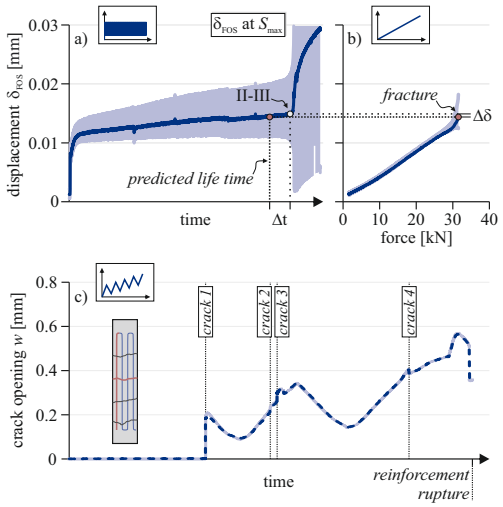

Fig. 13: Displacement progressions of a test under a) fatigue loading and b) monotonic loading, as well as c) comparison of crack opening over time determined using DFOS and DIC.

5.4.3 Measurement after macro-crack formation

The developed application concept ensures that the high-resolution characteristics of DFOS remain intact even after crack formation, enabling the use of measured strain data for crack width calculation throughout the entire loading process. The detailed relationships and boundary conditions governing crack width computation are

comprehensively discussed in [73]. For quantitative validation, crack widths calculated using DFOS were compared to those obtained through digital image correlation (DIC) (Figure 13c). Neither newly formed cracks within the measurement area nor large crack widths in later loading stages significantly impact the accuracy of crack width estimation. However, measurement accuracy is highly dependent on crack location. If a crack is situated near the edge of the measurement field, part of the increasing strain remains unrecorded, resulting in an underestimation of crack width. This highlights a key challenge in crack width computations using DFOS: when cracks form near the boundary of the measurement area – despite being within it – the available data points may be insufficient for accurate crack width determination.

A more in-depth analysis of the DFOS measurement capabilities following macro-crack formation lies beyond the scope of this article and is available in [73]. Nonetheless, it can be summarized that other influencing factors, such as strain-dependent debonding of the sensing fiber – also referred to as *capping* – or high cyclic loading, do not show a significant negative impact on the quality of crack width computation. In contrast, high loading frequencies (>1 Hz), which are commonly encountered in experimental fatigue research, present a significant challenge for strain measurements using DFOS.

5.4.4 Evaluation and Results

To enhance the application concept for two-dimensional strain field monitoring (2D-FOS), three independent sensor fibers were arranged in a grid-like pattern on the concrete surface (Figure 14a). The raw unidirectional strain data underwent filtering, downsampling, and segmentation [63], followed by interpolation and principal strain transformation to generate full-field two-dimensional strain profiles. These strain profiles were subsequently analyzed using the same algorithms developed for one-dimensional fiber segments, enabling both crack localization and the quantification of position-dependent crack widths at each measurement time step (Figure 14c-f).

To validate this approach, monotonic uniaxial tensile tests were conducted. The applied load and the final crack pattern, which comprises three cracks within the measurement field, are depicted in Figure 14b.Figures 14c–e illustrate the strain and crack profiles at the moments of crack formation, providing precise crack localization and enabling the quantification of position-dependent crack widths. These profiles exclusively consider strain components aligned with the loading direction, clearly revealing a slight eccentricity in the applied load. This effect is even more pronounced in the crack profiles, where one side consistently exhibits larger crack openings.

However, as previously noted, crack width estimation near the boundaries of the measurement field remains unreliable. While crack formation/position can still be identified, crack width computation in these regions is not feasible, and the corresponding areas are therefore left blank in the visualization.

Finally, Figure 14f presents strain and crack profiles at the peak load level. At this stage, the strain distribution becomes highly diffuse, making individual cracks difficult to distinguish. The crack profile, however, facilitates interpretation by revealing the onset of reinforcement yielding in Crack 2, which leads to a disproportionate increase in crack opening, ultimately resulting in failure.

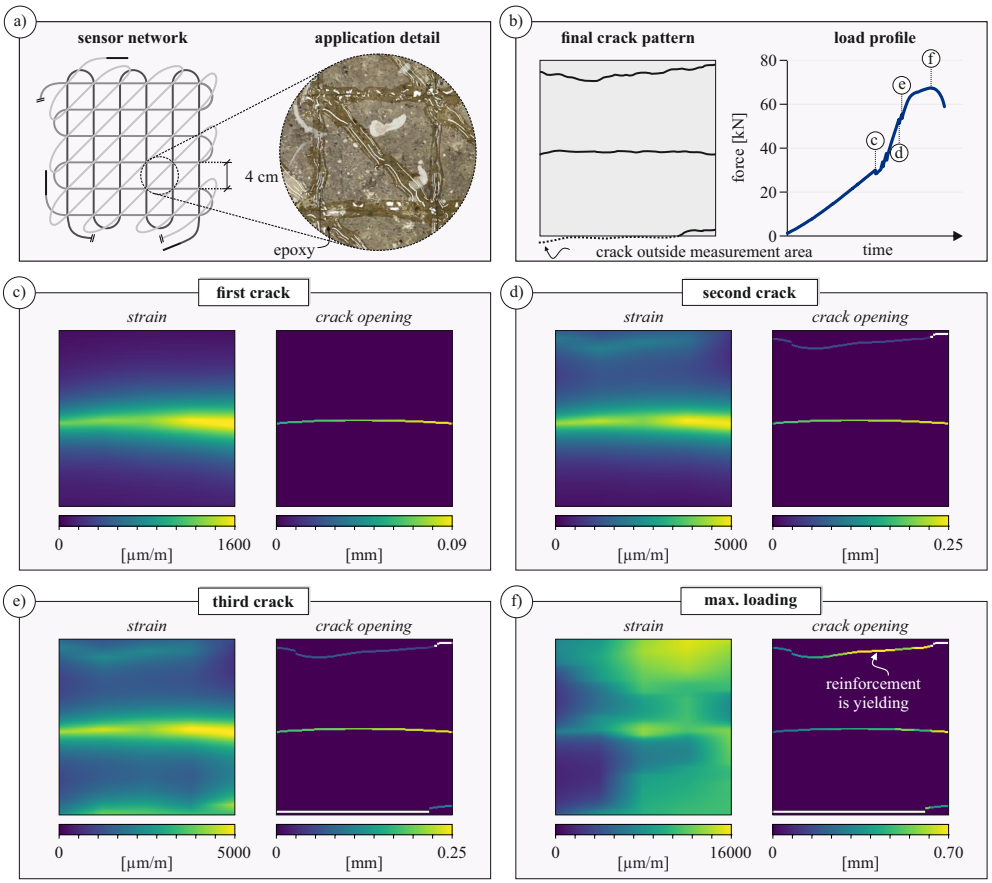

Fig. 14: 2D-FOS: a) Sensor network and detail, b) final crack pattern and load profile, as well as c–f) strain and crack profiles throughout the experiment.

The results indicate how 2D-FOS offers a significant advancement in shear monitoring of RC structures. By providing high-resolution, two-dimensional strain and crack width data, it enables both early-stage crack detection and long-term monitoring under repeated loading. The ability to accurately localize and quantify crack propagation enhances SHM capabilities, providing an additional tool for the assessment and maintenance of existing bridge structures. Currently, 2D-FOS is being further developed to compensate for the influence of temperature and to predict the remaining time until crack initiation based on the strain evolution. The deployment of the fiber grid on the Rhine River bridge "Nibelungenbrücke Worms" is planed.

5.5 Monitoring debonding of externally bonded CFRP strips with DFOS

Externally Bonded Reinforcement (EBR) made of CFRP is widely used for the strengthening of degraded concrete components because of its high strength, lightweight and simplicity of application. Retrofitting involves the external bonding of CFRP strips to the surface of existing concrete structures to increase their load-bearing capacity and extend their service life.

However, an intact adhesive bond between the concrete substrate and the CFRP strip is the basic requirement for the load-bearing capacity of the structures strengthened in this way. One of the most common forms of damage when using externally bonded reinforcement is debonding, in which the adhesively bonded reinforcement decouples due to cracking in the concrete substrate along the reinforcement. These damages in the bond interface caused by excessive loading accumulate and eventually lead to a sudden debonding failure of the CFRP reinforcement. In regard to this brittle failure mode of the bond interface, appropriate SHM concepts for measuring the load bearing behaviour of the CFRP reinforcement must be implemented, in order to prevent an unexpected collapse of the strengthened structures.

Strain measurements with distributed quasi-continuous DFOS are advantageous for monitoring and also for analyzing the adhesive bond properties. While common discrete strain measurement methods such as strain gauges can measure local strain at single spot accurately, but are often limited in their place of application [76]. For detecting cracks and especially the debonding of the EBR a more sophisticated measurement method is needed for SHM purposes.

In this case, DFOS can be integrated into the CFRP strips in order to capture the strain distribution along the entire length of the CFRP reinforcement. By using this state-of-the-art measurement method spatial resolution as low as 0.65 mm can be achieved in order to analyse the local bond properties in the joint interface. The local shear stress distribution can be derived from the DFOS strain measurement. Combining this with a suitable calculation method, the load-bearing capacity can be calculated and the decoupling process of the CFRP strip can be monitored accordingly in this way. In the following, the partial differential equation of the bonded joint, the derivation of the bond parameters and the possibilities of damage detection in EBR using DFOS are presented.

5.5.1 Characteristics of debonding of externally bonded CFRP strips

The reinforcement of concrete beams requires the transfer of forces between the concrete and the CFRP. This requires an intact bond and the avoidance of debonding. The failure modes of debonding in a reinforced concrete beam are categorised according to where the debonding starts. [77]. A distinction is made between *end anchorage debonding* and *intermediate crack debonding*. In the case of end anchorage debonding, the damage starts at the first bending crack and then progresses towards the support. The phenomenon of end anchorage debonding can be described by the differential equation of a bonded joint. In the case of intermediate crack debonding, the damage

starts in the middle of the beam between two cracks. Here the crack spacing and the forces acting on the cracks determine whether debonding will occur.

5.5.2 Measuring concept and damage detection

Generally, the bond of the externally bonded CFRP strip, especially at the end anchorage area, can be described by the partial differential equation of a bonded joint, see eq. 2.

$$\ddot{s_L} = \frac{1}{E_L \cdot t_L} \cdot \tau_L(s_L) \tag{2}$$

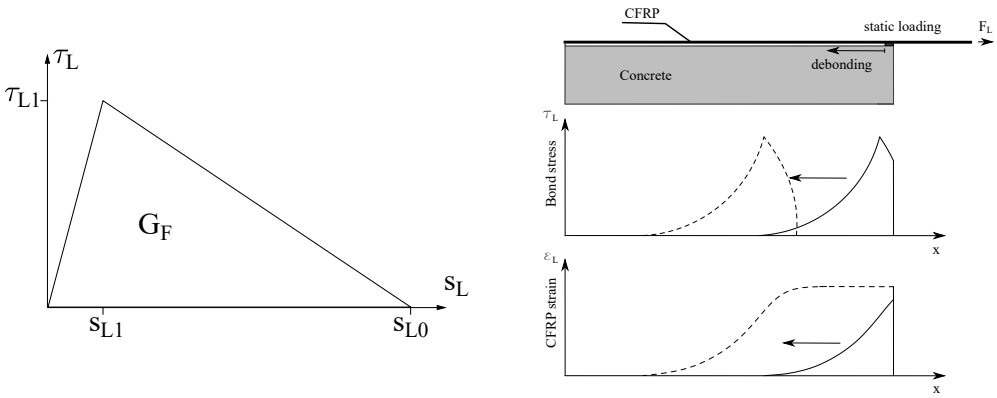

Fig. 15: Bilinear bond stress – slip $\tau_{L(s_L)}$ relationship (left), τ_L and ε_L distribution (right)

To solve the equation, a shape function for the relationship between bond stress and slip $\tau_{L(s_L)}$ is required. Depending on the slip s_L, the bond stress transfer can be described in 3 distinctive stages. At low loads, the bond between CFRP strip and the concrete substrate behaves almost linear elastically. After reaching the maximum bond stress τ_{L1} cracks start to develop inside the concrete substrate, which lead to a softening of the bond stress transfer. The debonding process is characterized by a successive decrease in the bond stress transfer. Eventually when the slip between the CFRP strip and the concrete substrate exceeds s_{L0}, the designated failure in form of "debonding" occurs, where the CFRP strip is detached from the concrete surface and the bond stress transfer is reduced to zero. The area of the $\tau_{L(s_L)}$ relationship is the bond fracture energy G_F, which is needed to obtain a complete decoupling of both materials. The aforementioned shape function can be described by a simplified bilinear model according to Holzenkämpfer [78], see Figure 15 (left) and the bond stress τ_L and CFRP strain ε_L distribution along the bonded length according to the $\tau_{L(s_L)}$ constitutive law is shown in Figure 15 (right). The significant parameters of the bond stress-slip relationship such as the maximum bond stress τ_{L1} and the corresponding

slip s_{L1} as well as the maximum slip value s_{L0} can be assessed by experimental studies conducted with DFOS measurements.

The second type of debonding failure mode is the intermediate crack debonding. The debonding process is initiated at intermediate flexural cracks in the concrete member. Softening failure is caused by exceeding the maximum transferable bond force ΔF_L in the concrete substrate between two adjacent intermediate cracks. This failure mode is usually indicated as intermediate crack debonding [77]. According to the german guideline DAfStb (2012) [79] the bond force ΔF_L between two adjutant cracks must be limited. The maximum resistance value of $\Delta F_{L,Rd}$ depends on the bond constitutive law $\tau_{L(s_L)}$, on the distance between the cracks s_r and on the force F_L in the CFRP reinforcement [77].

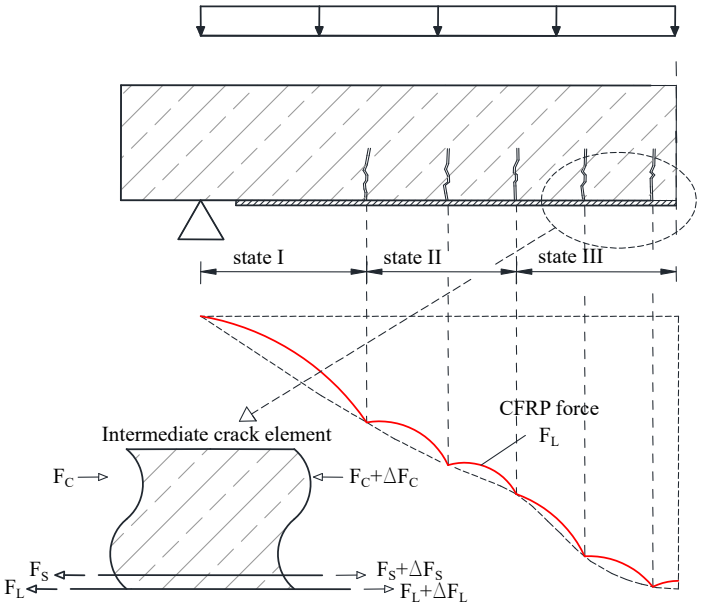

Fig. 16: Intermediate cracks of the strengthened flexural RC member [80]

5.5.3 Evaluation and Results

In order to describe the bond behaviour of the externally bonded CFRP strip, experimental tests must be carried out to determine the bond parameters. The input parameters are derived from experimental tests including *double lap shear tests* and *large scaled bending tests* on strengthened concrete components. The methodology of the tests is based on conventional testing methods in combination with DFOS. The parameter identification is evaluated from the measured DFOS data.

For the description of the CFRP bond interface in the end anchorage area, *tension-tension* double lap shear tests are carried out on strengthened concrete specimens (800 mm x 200 mm x 400 mm), which is separated horizontally into two equal parts by

a crack plate. Two CFRP strips with an average elastic modulus E_L of 170 000 MPa and a cross section A_L = 1.4 mm x 50 mm are applied on both sides of the roughened concrete surfaces. The adhesive used is a two-component epoxy resin. The thickness of the adhesive layer is set to 1 mm. The strain development of the CFRP strips is measured with quasi-continuously with fibre optic sensors. The shear test was carried out until the CFRP strip failed to debonding. The strain development during the experiment tests was recorded using a DFOS measurement system (LUNA ODISi 6000), where the spatial resolution of each measurement points is set to 0.65 mm. The test setup of the the double lap shear test is shown in Figure 17.

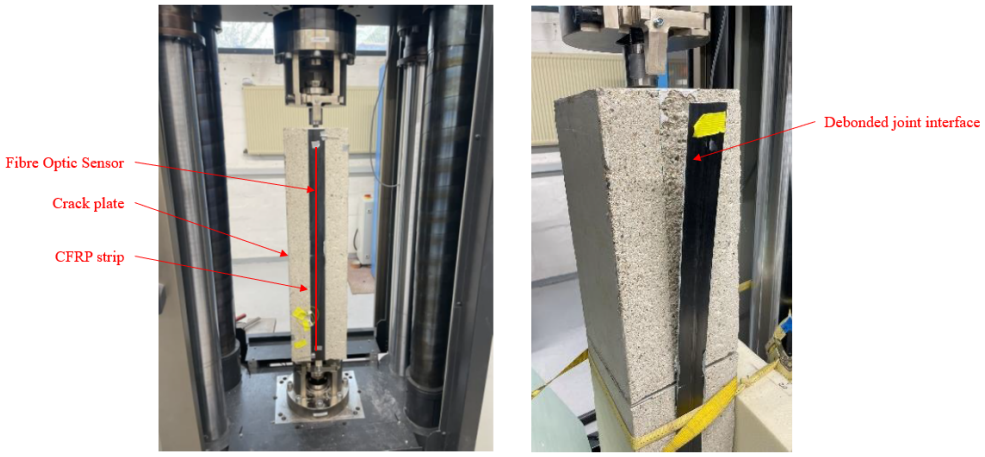

Fig. 17: Test setup of the double lap shear test

In order to investigate the IC debonding failure, experimental tests were conducted on large scaled RC slabs strengthened with externally bonded CFRP strips using DFOS to capture the strain distribution between the intermediate cracks. Reinforced concrete slabs are tested in a four-point bending static loading test, as shown in Figure 18. The test specimens have a length l = 3.2 m, a width b = 30 cm and a height h = 15 cm. The externally bonded CFRP strips have a length L = 3 m and a cross section A_L of 1.4 x 50 mm^2 and the steel rebars have a diameter d_s = 12 mm. The thickness of the concrete cover is set to 20 mm. The experimental tests are performed in a hydraulic testing machine, where the load is applied with a constant displacement rate of 0.03 mm/s until debonding failure of the EBR. The quasi-continuous strain measurement of the externally bonded CFRP strip is carried out by using distributed fibre optic sensor along the entire lengths of the CFRP reinforcement, which is mounted onto the exterior surface of the EBR. The fibre optic sensor is covered with an additional layer of epoxy resin in order to ensure protection and enhance the bond between the sensor and the surface.

Strain measurements with DFOS allow direct conclusions to be drawn about the debonding behaviour of the CFRP strips. The bond parameters can be derived from the strain curves that are measured on the double shear tests. The forces in the bonded

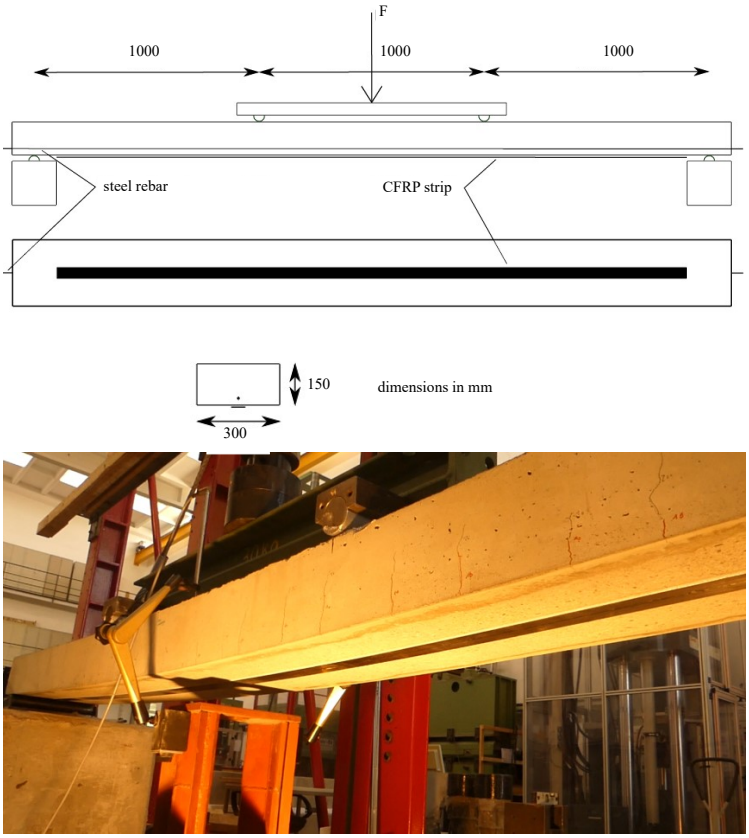

Fig. 18: Test setup of large scaled four-point bending test with DFOS

reinforcement can be derived directly from the strain measurement on the bending beam.

The strain distribution along the adhesive length at different load stages measured with DFOS is shown in Figure 19.

At early load stages, strains start to develop at the loaded end of the CFRP strip until a maximum force is reached. Upon increasing displacement, the s-shaped strain curve starts to move towards the unloaded end, due to crack-induced softening and debonding in the concrete bond interface. At the same time, the strain distribution at the loaded end forms a constant plateau when the maximum slip s_{L0} is exceeded and local debonding occurs. The debonding progresses gradually towards the unloaded end, until the remaining bond length left is insufficient to withstand the applied bond forces and a sudden bond failure is obtained.

Using the recorded DFOS measurement, the bond parameters τ_{L1}, s_{L0} and s_{L0} needed to describe the $\tau_{L(s_L)}$ relationship can be obtained with the *Method of Least Squares* [81]. The partial differential equation 2 can be solved using numerical procedure based on finite difference method to calculate the bond stress τ_{Li} , the slip s_{Li}

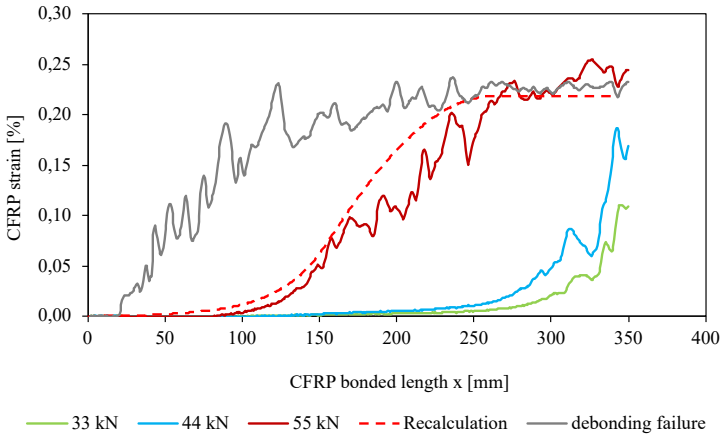

Fig. 19: Strain development along the CFRP strip during the experimental test at different load stages measured with DFOS

and the local strain ε_{Li} on each differential bond element with a spatial discretizations size d_x equals to 0.65 mm. The recalculation of the CFRP strain upon reaching 55 kN is shown in Figure 19.

Areas susceptible to debonding can be identified from the strain distribution on the strengthened RC beam measured by DFOS. The strain distribution of the CFRP strip at different load stages recorded with DFOS is shown in Figure 21. At initial load stage the DFOS measurement is able to capture the early flexural crack formation in the concrete slab, which is indicated by the local strain spikes. The position and the spacing between the flexural cracks s_r are crucial for the determination of the force distribution in the intermediate crack elements. It can be observed, that the strain development between the adjutant cracks is lower than the strain at the crack opening, due to bond stress transfer into the concrete.

Upon increasing loads, the difference of the CFRP strain at the upper and lower loaded crack increases, which corresponds to the increase of the force difference ΔF_L, as shown at the second intermediate crack element next to the end anchorage in Figure 21. If ΔF_L exceeds the maximum resistance $\Delta F_{L,Rd}$ an intermediate crack debonding is obtained.

For structural health monitoring purposes, the force difference ΔF_L between the intermediate cracks can be derived from the DFOS strain measurement. The position of critical intermediate crack elements can be localised by comparing the force differences ΔF_L with the maximum bond force $\Delta F_{L,Rd}$ between the respective cracks. These locations should then be observed more closely to avoid debonding failure.

The investigations have shown that DFOS is suitable for the identification of bond parameters. In addition, the critical locations for bond failure can be identified on an EBR-reinforced concrete member. However, for long-term monitoring, time-dependent effects such as bond creep and the associated redistribution of forces from the bonded to the embedded reinforcement still need to be taken into account.

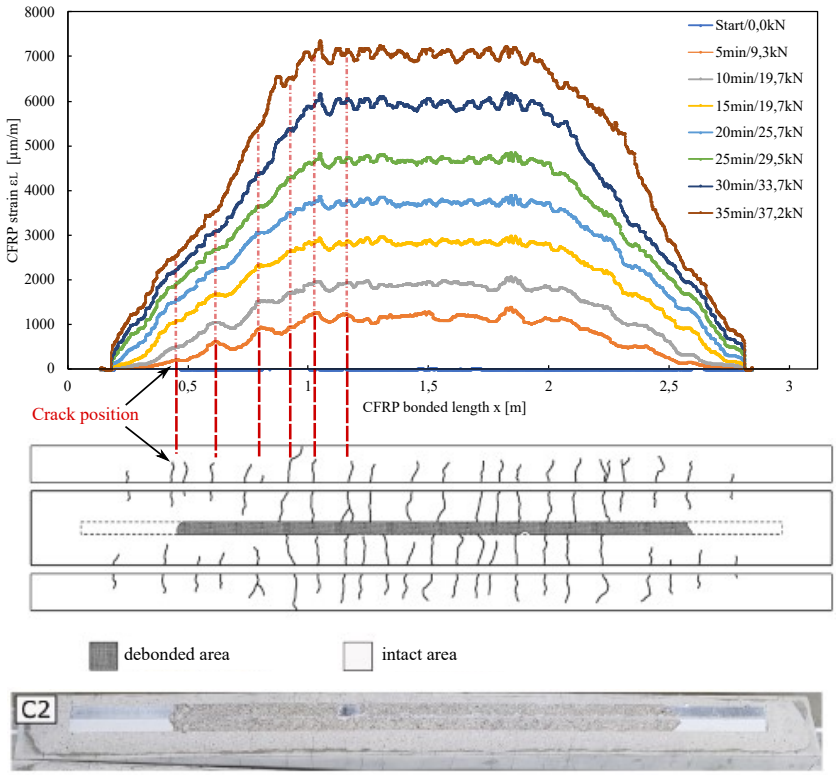

Fig. 20: Strain distribution of the RC slab at different load stages

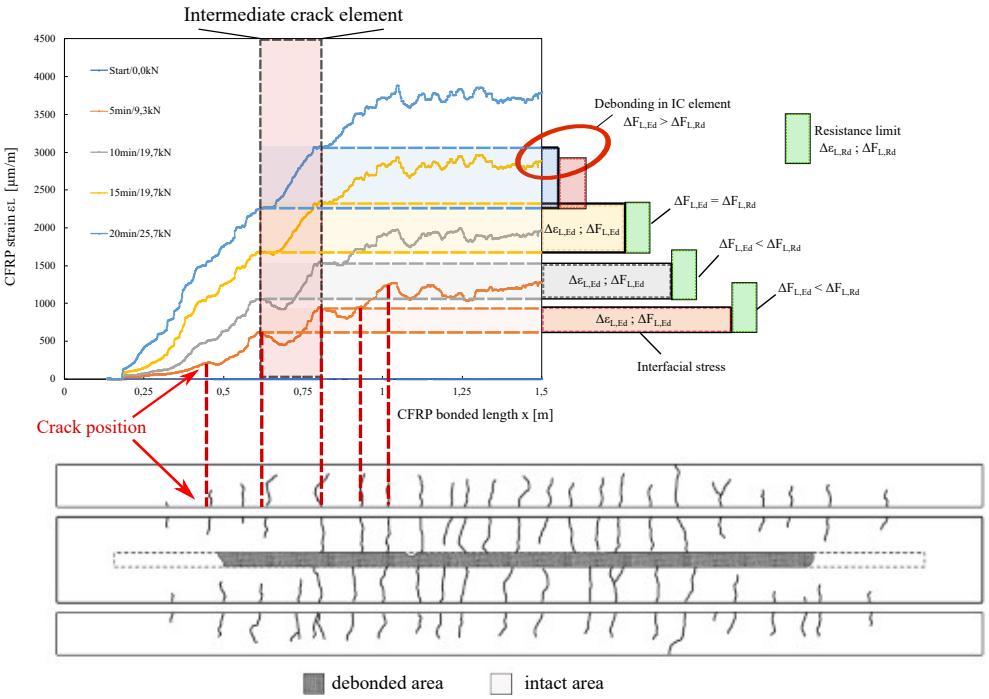

Fig. 21: Strain distribution of the RC slab at intermediate crack element

5.6 Linkage of multi-scale sensor data in a component test

5.6.1 Characteristics of damage

Linking different sensor types on multi-geometrical and multi-temporal scale allows to enhancement damage identification [71, 82]. Results for damage localization from system identification with Operational Modal Analysis (OMA) of data from acceleration sensors on a global geometrical scale will help to apply methods an local scale like Acoustic Emission (AE) and Impact-Echo more efficient. Methods which work on both scales like DIC (full-field displacement) and DFOS (strain along the fiber or fiber grids) , depending on resolution and sensor placement, are helpful to link methods of multi-geometrical scale. To investigate the fusion of different sensor data, a component test was designed that should mimic a part of a hollow box cross section of a concrete bridge. For a sensitivity test of the various testing methods, a gradual damage is applied to the structure, while the monitoring system was running to record several parameters of the structure.

5.6.2 Measuring concept and damage detection

The Modal Analysis with Stochastic Subspace Identification is used to detect global damage, if so, to characterize, localize and quantify the damage [83]. The detection and quantification is possible due to differential measurements to an initial state (undamaged or already damaged). If there is a change in structural stiffness there will be a drop in the Eigenfrequencies of the several Eigenmodes (mass is considered constant) [84]. Since the Eigenfrequencies of the several modes are different influenced by the type of damage, one can also characterize the damage with some knowledge about the mode shapes, but localization is not as trivial. Therefore, the method of the Modal Strain Energy for plate-like structures [85] was modified. Based on the identified modal parameters, it uses the local changes of the elastic strain energy of the mode shapes to localize these changes in stiffness which is considered as damage. To get some more support points for the analysis, a 2D Spline interpolation is interposed [86].

The drop in the average Eigenfrequency should be equivalent to the reduction in stiffness. To validate this, an energy-based method which is also based on elastic waves, the AE is used [87]. In difference to the already applied AE on tendons in prestressed concrete, here the AE is monitoring the reinforced concrete component and sensing the structure-borne sound induced by the opening cracks.

5.6.3 Experimental setup of the component test

The experimental investigation is carried out on a wall-like precast reinforced concrete component, which represents a section of a bridge box. The component is made of reinforced C30/37. The wall is 1.8 m high, 1 m wide and 15 cm thick. The base has a height of 20 cm. The component has a mass of approx. 1 tonne. The structure is equipped with a grid of 32 uniaxial piezoelectric acceleration sensors (Figure 22) for the Operational Modal Analysis as well as acoustic emission sensors to track and quantify the crack formation over time during the damage [84].

In addition, optical measurement methods (DIC) are used to capture the displacement fields and crack propagation, as well as DFOS to detect small strains in the early crack stage. The structure is held in a loading phase with crossbeams at the top and bottom and a point load is applied in the center by a hydraulic cylinder for gradual damage. For vibration measurement, the loading device is dismantled and the structure is excited with an impulse hammer while the data acquisition is running. This procedure is repeated for each load level (0 kN to 160 kN in 10 kN steps) with gradual increase in damage Figure 23. Since in a previous test early crack formation was recognized, additionally DFOS was added to the surface. DIC was used for validation and monitoring the opening of the cracks. Also an strain gauge was added to validate the measurement at least in one point.Figure 24

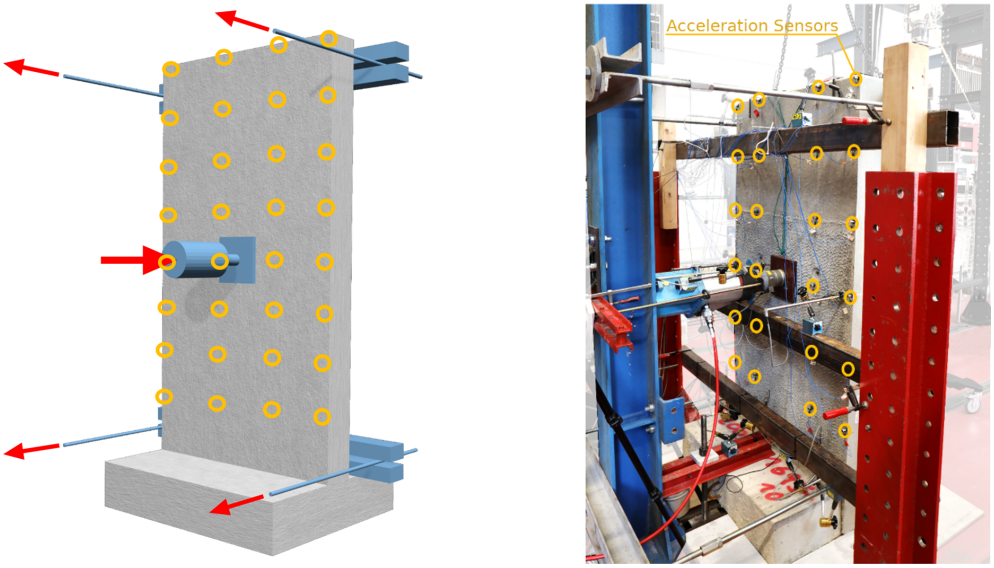

Fig. 22: left: Diagram with acceleration sensor grid, right: Photo of test setup

5.6.4 Brief conclusion of the component test

The strain measurement for DFOS and DIC showed good consistency. The DFOS was much more sensitive for early and pre-crack stage. But with increasing crack width, the DFOS could not read values for regions with high strain gradients, although the fibres did not brake. So the opened crack could be better observed by DIC, so both methods added well [71, 82, 84].

With the four acoustic emission sensors the cracks could be localized. The crack events are shown on the crack pattern recorded with DIC. Interestingly the AE crack localization is ahead of the manifested cracks observed on the surface (see red dots at load stage 80 kN in the subsequent crack area in Figure 25).

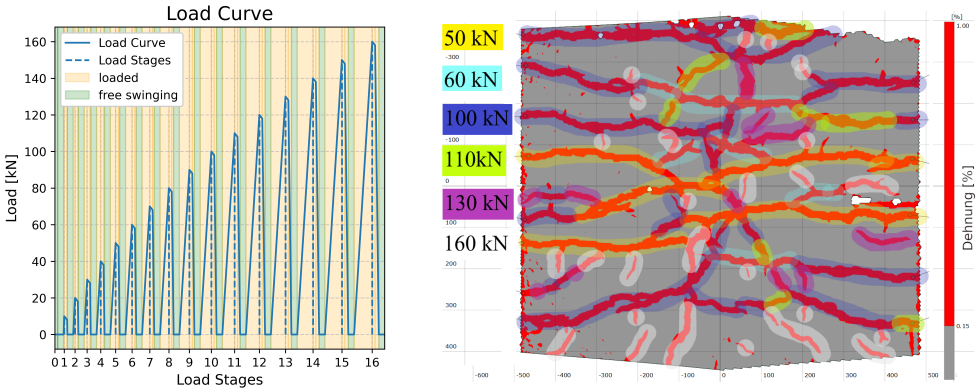

Fig. 23: left: Load stages during the test, right: Crack pattern after selected load stages

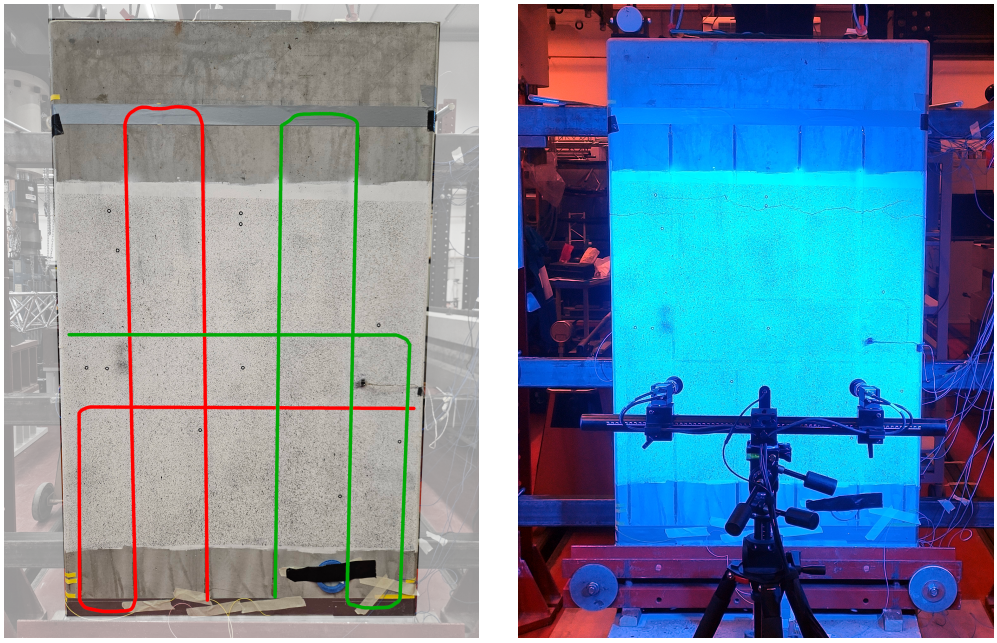

Fig. 24: left: DFOS sensors, right: DIC system Zeiss Aramis

For the linkage of different sensors of global and local scale an energy-based approach is applied. As reference points the undamaged and the highest damage of load stage 160 kN is used. The cummalive energy of the crack events is compared to the stiffness loss of the structure measured by the shift of the Eigenfrequency (Figure 26). As it can be seen this approach works well, further methods should be included in the comparison.

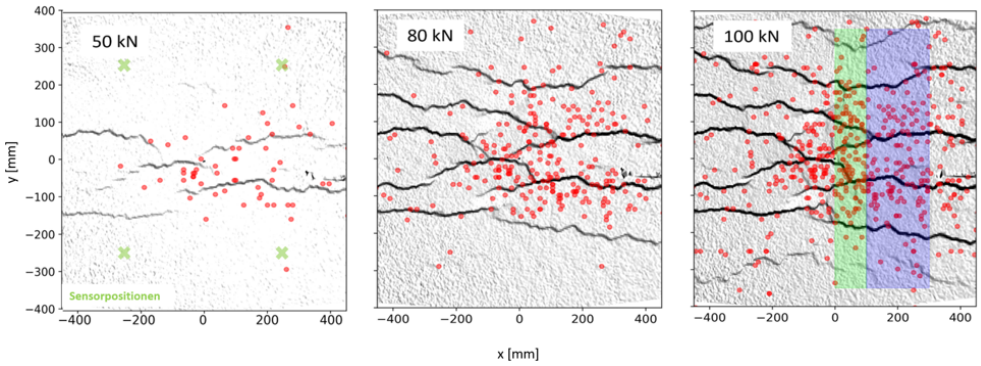

Fig. 25: Localized **AC!** (**AC!**) crack events (red dots) an DIC crack pattern for three load stages (50kN, 80 kN, 100 kN)

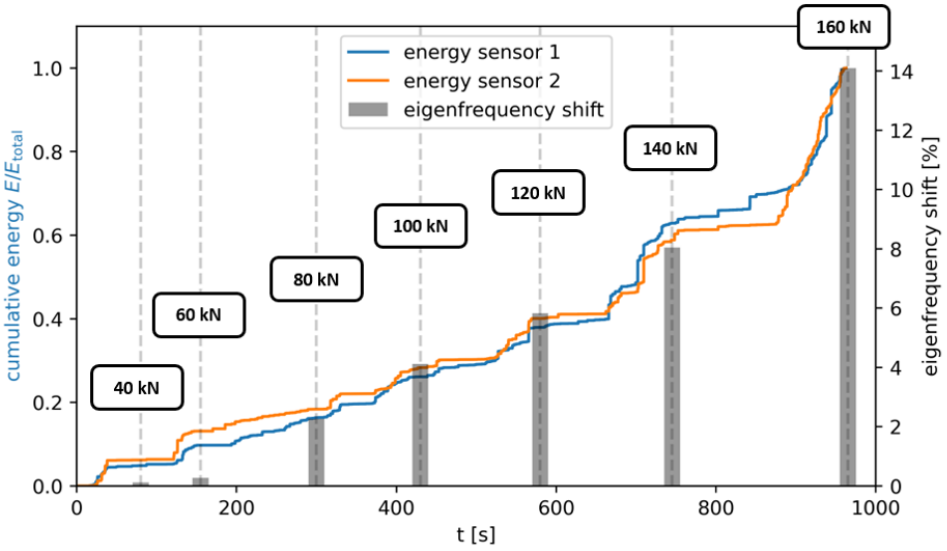

Fig. 26: Fracture energy vs. shift in Eigenfrequency

6 Discussion

The present methods demonstrate the broad applicability of enhanced DFOS for monitoring a variety of damage types on bridges:

Bond-failure monitoring was achieved by embedding a fiber directly in the reinforcement (steel or GFRP). The sensor records the strain transfer between the bar and the surrounding concrete, allowing the detection of debonding events; the sensitivity of this approach depends on the adhesive used and on the fiber coating. Surface crack detection was performed with fibers placed inside the concrete matrix. Because the sensors are protected from weathering and mechanical impact, they can reliably locate cracks and estimate their opening width. However, the correlation between the internal strain peak and the external crack geometry must still be verified for complex bridge geometries and variable loading conditions.

Two-dimensional DFOS (2D-DFOS) grids were employed to capture strain fields associated with internal tendon breaks and shear failure of reinforced concrete members. Artificial tendon ruptures generated distinct strain patterns on the concrete surface, yet these patterns can be obscured by overlapping load components, making detection more difficult. Shear-monitoring with 2D-DFOS enables early-stage crack identification and long-term observation under repeated loading, although crack width estimation near the edges of the measurement area remains uncertain. Current research therefore focuses on temperature compensation and on developing predictive models that relate strain evolution to the remaining service life before crack initiation.

2D-DFOS already allows with just one grid configuration the assessment of several damage types, such as shear, tendon rupture, and crack formation. The linkage of DFOS with other sensor data (accelerometers, umidity sensors) could help to differentiate between damage types or complex loading environments.

The debonding of externally bonded CFRP strips was investigated. DFOS proved capable of locating critical bond-stress zones on externally bonded-reinforced concrete members, but long-term monitoring must account for time-dependent phenomena such as bond creep and the gradual redistribution of forces from the external to the internal reinforcement.

Practical deployment of DFOS also encounters technical constraints. The usable length of DFOS with Rayleigh-backscatter is limited to about 100 m (∼250 m with an extender). Whereas Brillouin-based interrogation can reach longer distances at the expense of spatial resolution and in general long measurement times as well as the absence of true dynamic capability. The difficulty of constructing large-area 2-D-FOS networks further restrict current applications. For new constructions, fibers can be cast within the concrete or embedded into reinforcement, but questions remain regarding long-term durability, signal stability, and the possibility of replacement over bidge service live. Robust system design therefore requires redundancy (e.g., parallel fiber routes, protected connectors) to mitigate failures caused by fiber breakage, cable damage, or connector loss. Efficient data-analysis pipelines and data-reduction strategies are also essential to handle the massive volumes of distributed strain data generated during continuous monitoring.

The concepts presented still need to be validated under real world conditions. Several platforms are available: The existing concrete bridge *Niebelungenbrücke Worms*

was equipped with a heterogeneous SHM suite (humidity, temperature, displacement-transducers, and acceleration sensors) and will be expanded with line-wise DFOS and 2D-DFOS grids to assess sensor performance under realistic traffic, environmental loading conditions [88]. An other Platform is the IDA-KI "open-lab" bridge—a 45-m-long prestressed-concrete test structure incorporating typical structural deficiencies and sensor faults—hosts a comprehensive fiber-optic and electrical sensor network. This laboratory bridge serves as a benchmark for evaluating damage-detection algorithms, data-fusion strategies, and the robustness of DFOS under high damage-rate scenarios that would be unacceptable in bridges under service [89].

However, systematic investigations on DFOS are still lacking in the case of steel bridges. The challenges that must be addressed are related to geometric and surface constraints. In the context of steel structures, it is required that fibers be bonded to the surface. The quantification of the influence of coating systems on bridges has not been performed. Damage to steel structures is typically characterized by the presence of cracks in welds, which are associated with low radii, where fibers can just limited be applied. Consequently, the monitoring of damages on steel bridges with DFOS has to be performed indirectly, thus necessitating the development of novel methodologies for the placement of sensors and data analysis. However, the benefits that were exhibited by DFOS through the various applications on concrete bridges suggest that new strategies for monitoring steel structures are also on the horizon.

7 Conclusion

Distributed Fiber-Optic Sensing is emerging as a standard tool for SHM of concrete bridges and has great potential for steel bridges, as well. Its ability to deliver quasi continuous strain and temperature monitoring along the fiber with high spatial resolution and strong environmental robustness opens new perspectives for safety management and asset-maintenance. Although the technology currently suffers from high initial costs and a number of technical challenges, ongoing advances in methods are expected to reduce these barriers. Consequently, DFOS is likely to play an increasingly important role in the monitoring of bridges.

Realizing this potential will require coordinated progress on several fronts:

1. **Standardised installation and bonding procedures** for both, new and existing bridges.
2. **Durable sensor designs and redundant architectures** that ensure long-term signal stability despite mechanical damage or environmental exposure.
3. **Multi-sensor fusion and data visualisation** integration of DFOS data with complementary point sensors and with remote-sensing modalities to obtain a holistic view of bridge behaviour, interactive visualisation platforms are essential for predictive maintenance and decision-making.
4. **Systematic, full-scale validation on a variety of bridge types** (concrete, prestressed, orthotropic steel decks, etc.) to demonstrate reliability under realistic traffic and climatic conditions.

Addressing these challenges will transform DFOS from a promising research instrument into a cornerstone of enhanced SHM strategies, delivering earlier damage detection, more accurate condition assessment, and ultimately safer and more efficient bridge management.

Declaration of Competing Interest

The authors declare that they have no known competing financial interests or personal relationships that could have appeared to influence the work reported in this paper.

Declaration of generative AI and AI-assisted technologies in the writing process

During the preparation of this work the authors used ChatGPT (based on GPT-5 -OpenAI) in order to reorganize the notes and improve the manuscript readability. After using this tool/service, the authors reviewed and edited the content as needed and take full responsibility for the content of the published article.

Funding

The research presented in this paper is being conducted within the Cluster "Damage detection", part of the Priority Programme SPP 2388 "Hundred plus - Extending the Lifetime of Complex Engineering Structures through Intelligent Digitalization", funded by the Deutsche Forschungsgemeinschaft (DFG, German Research Foundation) - project number 461030501. Contributing projects are: 501805504, 501823987, 501808860, 501771082, 501798687, 501774158.

Data availability

Data will be made available on request.

CRediT authorship contribution statement

Julian Unglaub contributed Writing – original draft, Conceptualization, Funding acquisition and Supervision; Aeneas Paul contributed Writing – original draft, Investigation, Visualization and Formal analysis; Henrik Becks contributed Writing – original draft, Investigation, Visualization and Formal analysis; Zhuo Chen contributed Writing – original draft, Investigation, Visualization and Formal analysis; Chongjie Kang contributed Writing – original draft, Investigation, Visualization and Formal analysis; Paul Winkler contributed Writing – original draft, Investigation, Visualization and Formal analysis; David Sanio contributed Writing – original draft, Conceptualization, Funding acquisition and Supervision; Carsten Könke contributed Writing – review & editing, Conceptualization, Funding acquisition and Supervision; Thorsten Leusmann contributed Writing – review & editing, Conceptualization, Funding acquisition and

Supervision; Josef Hegger contributed Writing – review & editing, Conceptualization, Funding acquisition and Supervision; Dirk Lowke contributed Writing – review & editing, Conceptualization, Funding acquisition and Supervision; Martin Classen contributed Writing – review & editing, Conceptualization, Funding acquisition and Supervision; and Steffen Marx contributed Writing – review & editing, Conceptualization, Funding acquisition and Supervision. All authors have read and approved the final manuscript.

References

[1] Li, H.-N., Li, D.-S., Song, G.-B.: Recent applications of fiber optic sensors to health monitoring in civil engineering. Engineering Structures **26**(11), 1647–1657 (2004) https://doi.org/10.1016/j.engstruct.2004.05.018

[2] Herbers, M., Richter, B., Marx, S.: Rayleigh-based crack monitoring with distributed fiber optic sensors: experimental study on the interaction of spatial resolution and sensor type. Journal of Civil Structural Health Monitoring (2024) https://doi.org/10.1007/s13349-024-00896-5

[3] Udd, E.: An overview of fiber-optic sensors. Review of Scientific Instruments **66**(8), 4015–4030 (1995) https://doi.org/10.1063/1.1145411

[4] Kersey, A.D.: A review of recent developments in fiber optic sensor technology. Optical Fiber Technology **2**(3), 291–317 (1996) https://doi.org/10.1006/ofte.1996.0036

[5] Grattan, K.T.V., Sun, T.: Fiber optic sensor technology: an overview. Sensors and Actuators A: Physical **82**(1-3), 40–61 (2000) https://doi.org/10.1016/S0924-4247(99)00368-4

[6] Lee, B.: Review of the present status of optical fiber sensors. Optical Fiber Technology **9**(2), 57–79 (2003) https://doi.org/10.1016/S1068-5200(02)00527-8

[7] Schnellenbach-Held, M., Peeters, M., Scheerbaum, F.: State of Strengthening Methods - Strengthening of Existing Concrete Bridges: Bericht zum Forschungsprojekt 89.217/2008/AP. Berichte der Bundesanstalt für Strassenwesen B, Brücken- und Ingenieurbau, vol. 75. Wirtschaftsverl. NW Verl. für neue Wiss, Bremerhaven (2010). https://bast.opus.hbz-nrw.de/frontdoor/deliver/index/docId/260/file/B75.pdf Accessed 22.09.2025

[8] Geißler, K.: Handbuch brückenbau: Entwurf, konstruktion, berechnung, bewertung und ertüchtigung. In: Geißler, K. (ed.) Handbuch Brückenbau, pp. 1135–1285 (2014). https://doi.org/10.1002/9783433603437.ch7

[9] Kovler, K., Chernov, V.: Types of damage in concrete structures. In: Failure, Distress and Repair of Concrete Structures, pp. 32–56. Elsevier, ??? (2009). https://doi.org/10.1533/9781845697037.1.32

[10] Robuschi, S., Ivanov, O.L., Geiker, M., Fernandez, I., Lundgren, K.: Impact of cracks on distribution of chloride-induced reinforcement corrosion. Materials and Structures **56**(1) (2023) https://doi.org/10.1617/s11527-022-02085-6

[11] Richter, B., Will, E., Herbers, M., Marx, S.: Detection of prestressing wire breaks in post-tensioned concrete structures using distributed fiber optic strain sensing. Journal of Civil Structural Health Monitoring (2025) https://doi.org/10.1007/s13349-025-01018-5

[12] Ruano, G., Quintana, V., La Scala, A., Foti, D.: On the effect of thermal strains in slender prestressed concrete beams. Materials and Structures **58**(7) (2025) https://doi.org/10.1617/s11527-025-02739-1

[13] Wetzel, T., Albrecht, F.: On the stepwise dismantling of concrete bridges with stress-corrosion-cracking-sensitive prestressing steel. Beton- und Stahlbetonbau **120**(2), 89–99 (2025) https://doi.org/10.1002/best.202400091

[14] Wang, L., Su, X., Ma, Y., Deng, M., Zhang, J., Cai, C.S.: Strengthening of steel decks for cable-stayed bridge using ultra-high performance concrete: A case study. Advances in Structural Engineering **23**(16), 3373–3384 (2020) https://doi.org/10.1177/1369433220939210

[15] Miki, C.: Retrofitting Engineering for Fatigue Damaged Steel Structures. Springer Nature Switzerland, Cham (2025). https://doi.org/10.1007/978-3-031-80146-4

[16] Rodriguez, G., Casas, J.R., Villalba, S.: Shm by dofs in civil engineering: a review. Structural Monitoring and Maintenance **2**(4), 357–382 (2015) https://doi.org/10.12989/smm.2015.2.4.357

[17] Barrias, A., Casas, J.R., Villalba, S.: A review of distributed optical fiber sensors for civil engineering applications. Sensors **16**(5) (2016) https://doi.org/10.3390/s16050748

[18] Bado, M.F., Casas, J.R.: A review of recent distributed optical fiber sensors applications for civil engineering structural health monitoring. Sensors **21**(5) (2021) https://doi.org/10.3390/s21051818

[19] Gowshikan, A., Kariyawasam, K., Xu, X., Kechavarzi, C., Battista, N., Ferdinando, N., Acikgoz, S., Gunawardana, N.D., Ranasinghe, M.: A review on the advances in distributed fibre optic sensing technology for structural health monitoring. In: Dissanayake, R. (ed.) 12th International Conference on Structural Engineering and Construction Management. Lecture Notes in Civil Engineering Series, vol. 266, pp. 145–159. Springer, Singapore (2023). https://doi.org/10.1007/978-981-19-2886-4

[20] Howiacki, T., Sieńko, R., Bednarski, Ł., Zuziak, K.: Structural monitoring of concrete, steel, and composite bridges in poland with distributed fibre optic

sensors. Structure and Infrastructure Engineering **20**(7-8), 1213–1229 (2024) https://doi.org/10.1080/15732479.2023.2230558

[21] Rodriguez, G., Casas, J.R., Barrias, A.: Monitoring of shear cracking in partially prestressed concrete beams by distributed optical fiber sensors. Proceedings of the 8th International Conference on Bridge Maintenance, Safety and Management, IABMAS 2016 (26–30 June 2016.)

[22] Barrias, A., Rodriguez, G., Casas, J.R., Villalba, S.: Application of distributed optical fiber sensors for the health monitoring of two real structures in barcelona. Structure and Infrastructure Engineering **14**(7), 967–985 (2018) https://doi.org/10.1080/15732479.2018.1438479

[23] Ye, C., Butler, L.J., Elshafie, M.Z.E.B., Middleton, C.R.: Evaluating prestress losses in a prestressed concrete girder railway bridge using distributed and discrete fibre optic sensors. Construction and Building Materials **247**, 118518 (2020) https://doi.org/10.1016/j.conbuildmat.2020.118518

[24] Glisic, B., Chen, J., Hubbell, D.: Streicker bridge: a comparison between bragg-grating long-gauge strain and temperature sensors and brillouin scattering-based distributed strain and temperature sensors. In: Tomizuka, M. (ed.) Sensors and Smart Structures Technologies for Civil, Mechanical, and Aerospace Systems 2011. SPIE Proceedings, p. 79812. SPIE, ??? (2011). https://doi.org/10.1117/12.881818

[25] Bastianini, F., Matta, F., Rizzo, A., Galati, N., Nanni, A.: Overview of recent bridge monitoring applications using distributed brillouin fiber optic sensors. e-Journal of Nondestructive Testing (2006)

[26] Regier, R., Hoult, N.A.: Distributed strain behavior of a reinforced concrete bridge: Case study. Journal of Bridge Engineering **19**(12) (2014) https://doi.org/10.1061/(ASCE)BE.1943-5592.0000637

[27] Sieńko, R., Bednarski, Ł., Howiacki, T.: Smart composite rebars based on dfos technology as nervous system of hybrid footbridge deck: A case study. In: Rizzo, P., Milazzo, A. (eds.) European Workshop on Structural Health Monitoring. Lecture Notes in Civil Engineering, vol. 128, pp. 331–341. Springer International Publishing, Cham (2021). https://doi.org/10.1007/978-3-030-64908-1$\backslash$textunderscore

[28] Howiacki, T., Sieńko, R., Bednarski, Ł., Zuziak, K.: Crack shape coefficient: Comparison between different dfos tools embedded for crack monitoring in concrete. Sensors **23**(2) (2023) https://doi.org/10.3390/s23020566

[29] Burger, H., Tepho, T., Fischer, O., Schramm, N.: Performance assessment of existing prestressed concrete bridges utilizing distributed optical fiber sensors. In: Biondini, F., Frangopol, D.M. (eds.) Life-Cycle of Structures and Infrastructure

Systems, pp. 3134–3141. Taylor & Francis, ??? (2023). https://doi.org/10.1201/9781003323020-382

[30] Burger, H., Schramm, N., Kuhn, D., Tepho, T., Breitenbücher, P., Fischer, O.: Monitoring of the kreuzhofbrücken in munich at risk of stress corrosion cracking - conceptualisation and findings from experimental investigations. Beton- und Stahlbetonbau (2025) https://doi.org/10.1002/best.70031

[31] Novák, B., Stein, F., Reinhard, J., Dudonu, A.: Einsatz kontinuierlicher faseroptischer sensoren zum monitoring von bestandsbrücken. Beton- und Stahlbetonbau **116**(10), 718–726 (2021) https://doi.org/10.1002/best.202100070

[32] Webb, G.T., Vardanega, P.J., Hoult, N.A., Fidler, P.R.A., Bennett, P.J., Middleton, C.R.: Analysis of fiber-optic strain-monitoring data from a prestressed concrete bridge. Journal of Bridge Engineering **22**(5) (2017) https://doi.org/10.1061/(ASCE)BE.1943-5592.0000996

[33] Kishida, K., Aung, T.L., Lin, R.: Monitoring a railway bridge with distributed fiber optic sensing using specially installed fibers. Sensors **25**(1) (2024) https://doi.org/10.3390/s25010098

[34] Wu, R., Biondi, A., Cao, L., Gandhi, H., Abedin, S., Cui, G., Yu, T., Wang, X.: Composite bridge girders structure health monitoring based on the distributed fiber sensing textile. Sensors **23**(10) (2023) https://doi.org/10.3390/s23104856

[35] Bednarski, Ł., Sieńko, R., Howiacki, T., Zuziak, K.: The smart nervous system for cracked concrete structures: Theory, design, research, and field proof of monolithic dfos-based sensors. Sensors **22**(22) (2022) https://doi.org/10.3390/s22228713

[36] Strasser, L., Lienhart, W., Madeleine, W.: Static and dynamic bridge monitoring with distributed fiber optic sensing. Structural Health Monitoring 2023, Proceedings of the 14th International Workshop on Structural Health Monitoring, 1–8 (2023)

[37] Enckell, M., Glisic, B., Myrvoll, F., Bergstrand, B.: Evaluation of a large-scale bridge strain, temperature and crack monitoring with distributed fibre optic sensors. Journal of Civil Structural Health Monitoring **1**(1-2), 37–46 (2011) https://doi.org/10.1007/s13349-011-0004-x . Accessed 24.09.2025

[38] Roibert, A., Virlogeux, M., Fasquel, C., Maherault, J.-P.: Normandie bridge – fatigue analysis and innovative instrumentation of the orthotropic steel deck. In: IABSE Symposium, Istanbul 2023: Long Span Bridges. IABSE Reports, pp. 854–861. International Association for Bridge and Structural Engineering (IABSE)Zurich, Switzerland, ??? (2023). https://doi.org/10.2749/istanbul.2023.0854

[39] Cola, S., Bersan, S., Michielin, E., Pangop, F.T., Simonini, P., Schenato, L.,

Palmieri, L., Bergamo, O.: On distributed strains in a cfa pile via dfoss measurements and numerical analysis. In: Proceedings of the XVII European Conference on Soil Mechanics and Geotechnical Engineering: H. Geotechnical Engineering, Foundation of the Future, pp. 3508–3515. European Association of Geotechnical Engineers, Vienna, Austria (2019)

[40] Gillham, J., Sturm, R., Hoult, N.A., Bentz, E.C.: Measuring support reactions in a composite model bridge using distributed fiber optic sensing. Journal of Structural Engineering **149**(7) (2023) https://doi.org/10.1061/JSENDH.STENG-12151

[41] Barker, C., Woods, J., Hoult, N.A., Le, H., Tolikonda, V.: Pre- and post-rehabilitation monitoring of a steel railway bridge with distributed and discrete sensors. Journal of Bridge Engineering **27**(4) (2022) https://doi.org/10.1061/(ASCE)BE.1943-5592.0001847

[42] van der Kooi, K., Hoult, N.A., Le, H.: Monitoring an in-service railway bridge with a distributed fiber optic strain sensing system. Journal of Bridge Engineering **23**(10) (2018) https://doi.org/10.1061/(ASCE)BE.1943-5592.0001281

[43] Matta, F., Bastianini, F., Galati, N., Casadei, P., Nanni, A.: Distributed strain measurement in steel bridge with fiber optic sensors: Validation through diagnostic load test. Journal of Performance of Constructed Facilities **22**(4), 264–273 (2008) https://doi.org/10.1061/(ASCE)0887-3828(2008)22:4(264)

[44] Gómez-Martínez, R., Sánchez-García, R., Escobar-Sánchez, J.A., Arenas-García, L.M., Mendoza-Salas, M.A., Rosales-González, O.N.: Monitoring two cable-stayed bridges during load tests with fiber optics. Structures **33**, 4344–4358 (2021) https://doi.org/10.1016/j.istruc.2021.07.026

[45] Xu, J., Dong, Y., Zhang, Z., Li, S., He, S., Li, H.: Full scale strain monitoring of a suspension bridge using high performance distributed fiber optic sensors. Measurement Science and Technology **27**(12), 124017 (2016) https://doi.org/10.1088/0957-0233/27/12/124017

[46] Lee, S.C., Tee, B.P., Chong, M.F., Ku Mahamud, K.M.S., Mohamad, H.: Structural assessment for an old steel railway bridge under static and dynamic loads using fibre optic sensors. In: DeJong, M.J., Schooling, J.M., Viggiani, G.M.B. (eds.) International Conference on Smart Infrastructure and Construction 2019 (ICSIC), pp. 729–736. ICE Publishing, ??? (2019). https://doi.org/10.1680/icsic.64669.729

[47] Zhou, J., Kang, C., Peng, M., Stümpel, M., Marx, S.: Investigations on bond performances of gfrp/stainless steel reinforcements using distributed fiber optical sensors (dfoss). Journal of Building Engineering **75**, 106881 (2023) https://doi.org/10.1016/j.jobe.2023.106881

[48] Zhou, J., Zhao, J., Peng, M., Liebscher, M., Mechtcherine, V., Marx, S., Kang,

C.: Experimental investigation on the bond performance of a hybrid lap-spliced connection of gfrp and stainless steel bars in concrete. Cement and Concrete Composites **157**, 105952 (2025) https://doi.org/10.1016/j.cemconcomp.2025.105952

[49] Zhou, J., Zhao, J., Peng, M., Liebscher, M., Mechtcherine, V., Marx, S., Kang, C.: Experimental investigation on the bond performance of a hybrid lap-spliced connection of gfrp and stainless steel bars in concrete. Cement and Concrete Composites **157**, 105952 (2025) https://doi.org/10.1016/j.cemconcomp.2025.105952

[50] Sträter, N., Clauß, F., Ahrens, M.A., Mark, P.: Detection of tendon breaks in prestressed concrete structures using coda wave interferometry. Structural Concrete (2024) https://doi.org/10.1002/suco.202400680

[51] Käding, M., Schacht, G., Marx, S.: Acoustic emission analysis of a comprehensive database of wire breaks in prestressed concrete girders. Engineering Structures **270**, 114846 (2022) https://doi.org/10.1016/j.engstruct.2022.114846

[52] Heinrich, J., Maurer, R., Leckey, K., Müller, C.H., Ickstadt, K.: Detektieren ermüdungsbedingter spannstahlbrüche mittels rissmonitoring im versuch und am bauwerk. Bauingenieur **96**(03), 92–101 (2021)

[53] Nürnberger, U.: Corrosion induced failure mechanisms of prestressing steel. Materials and Corrosion **53**(8), 591–601 (2002) https://doi.org/cmvczc

[54] Paul, A., Sanio, D., Mark, P.: Detection of internal tendon breaks by fiber-optical measurements – influence of the re-anchoring behavior. Procedia Structural Integrity **64**, 1287–1294 (2024) https://doi.org/10.1016/j.prostr.2024.09.199

[55] Sanio, D., Alawieh, H., Bomholt, F., Daake, H., Prenting, A., Mark, P.: Temporary post-anchoring of bar tendons by bond – development of an anchoring system for transversely pre-stressed deck-slabs. Beton- und Stahlbetonbau **116**(10), 741–753 (2021) https://doi.org/10.1002/best.202100069

[56] Briere, V., Harries, K.A., Kasan, J., Hager, C.: Dilation behavior of seven-wire prestressing strand – the hoyer effect. Construction and Building Materials **40**, 650–658 (2013) https://doi.org/10.1016/j.conbuildmat.2012.11.064

[57] Sanio, D., Löschmann, J., Mark, P., Ahrens, M.A.: Bauwerksmessungen versus rechenkonzepte zur beurteilung von spannstahlermüdung in betonbrücken. Bautechnik **95**(2), 99–110 (2018) https://doi.org/10.1002/bate.201700092

[58] Paul, A., Sanio, D., Mark, P.: Detektion innerer spannstahlbrüche durch faseroptische messungen an betonoberflächen. Beton- und Stahlbetonbau (120) (2025) https://doi.org/10.1002/best.202400100

[59] Paul, A., Sanio, D., Mark, P.: Monitoring tendon breaks in concrete structures at different depths using distributed fiber optical sensors. e-Journal of

Nondestructive Testing **29**(7) (2024) https://doi.org/10.58286/29598

[60] Mata-Falcón, J., Haefliger, S., Lee, M., Galkovski, T., Gehri, N.: Combined application of distributed fibre optical and digital image correlation measurements to structural concrete experiments. Engineering Structures **225**, 111309 (2020) https://doi.org/10.1016/j.engstruct.2020.111309

[61] Richter, B., Herbers, M., Marx, S.: Towards an automated crack monitoring using distributed fiber optic sensors. ce/papers **6**(5), 635–643 (2023) https://doi.org/10.1002/cepa.2036

[62] Richter, B., Herbers, M., Marx, S.: Crack monitoring on concrete structures with distributed fiber optic sensors—toward automated data evaluation and assessment. Structural Concrete **25**(2), 1465–1480 (2024) https://doi.org/10.1002/suco.202300100

[63] Janiak, T., Becks, H., Camps, B., Classen, M., Hegger, J.: Evaluation of distributed fibre optic sensors in structural concrete. Materials and Structures **56**(9), 1–18 (2023) https://doi.org/10.1617/s11527-023-02222-9

[64] Clauß, F., Ahrens, M.A., Mark, P.: Thermo–mechanical experiments on reinforced concrete beams: Assessing thermal, mechanical, and mixed impacts on fiber optic measurements. Structural Concrete **23**(6), 3521–3537 (2022) https://doi.org/10.1002/suco.202100890

[65] Clauß, F., Löschmann, J., Ahrens, M.A., Mark, P.: Temperaturinduktion in betontragwerke. Beton- und Stahlbetonbau **116**(7), 539–550 (2021) https://doi.org/10.1002/best.202100010

[66] Bundesanstalt für Straßenwesen: Brückenstatistik. https://www.bast.de/DE/Ingenieurbau/Fachthemen/brueckenstatistik/bruecken_hidden_node.html Accessed 04.09.2024

[67] Bundesministerium für Verkehr, Bau und Stadtentwicklung Abteilung Straßenbau: Richtlinie zur Nachrechnung von Straßenbrücken im Bestand: Nachrechnungsrichtlinie, Bonn

[68] Deutsches Institut für Normung e.V.: Eurocode 2: Bemessung und Konstruktion von Stahlbeton- und Spannbetontragwerken – Teil 2: Betonbrücken – Bemessungs- und Konstruktionsregeln: Deutsche Fassung EN 1992-2:2005 + AC:2008. Beuth, Berlin (Dezember 2010)

[69] Hegger, J., Marzahn, G., Teworte, F., Herbrand, M.: Zur anwendung des hauptzugspannungskriteriums bei der nachrechnung bestehender spannbetonbrücken. Beton- und Stahlbetonbau **110**(2), 82–95 (2015) https://doi.org/10.1002/best.201400106

[70] Hillebrand, M., Teworte, F., Hegger, J.: Shear fatigue of prestressed i-beams with shear reinforcement. Structural Concrete **22**(2), 1085–1099 (2021) https://doi.org/10.1002/suco.202000187

[71] Becks, H., Lippold, L., Winkler, P., Moeller, M., Rohrer, M., Leusmann, T., Anton, D., Sprenger, B., Kähler, P., Rudenko, I., Andrés Arcones, D., Koutsourelakis, P.-S., Unger, J.F., Weiser, M., Petryna, Y., Schnellenbach-Held, M., Lowke, D., Wessels, H., Lenzen, A., Zabel, V., Könke, C., Claßen, M., Hegger, J.: Neuartige konzepte für die zustandsüberwachung und -analyse von brückenbauwerken – einblicke in das forschungsvorhaben spp100+. Bauingenieur **99**(10), 327–338 (2024) https://doi.org/10.37544/0005-6650-2024-10-63

[72] Becks, H., Hegger, J., Classen, M.: Measuring strain and crack evolution in reinforced concrete under monotonic and fatigue tension using fiber optic sensors. Procedia Structural Integrity **64**, 1279–1286 (2024) https://doi.org/10.1016/j.prostr.2024.09.197

[73] Becks, H., Högemann, M., Hegger, J., Classen, M.: Externally installed fiber optic sensors for strain and crack monitoring of reinforced concrete structures. Measurement (Elsevier), (2025)

[74] Swaddiwudhipong, S., Lu, H.-R., Wee, T.-H.: Direct tension test and tensile strain capacity of concrete at early age. Cement and Concrete Research **33**(12), 2077–2084 (2003) https://doi.org/10.1016/S0008-8846(03)00231-X

[75] Thun, H., Ohlsson, U., Elfgren, L.: A deformation criterion for fatigue of concrete in tension. Structural Concrete **12**(3), 187–197 (2011) https://doi.org/10.1002/suco.201100013

[76] Chen, Z., Grefe, H., Leusmann, T., Dilger, K., Lowke, D.: Quasi-continuous strain measurement with distributed fibre optic sensors in reinforcement bars and externally bonded cfrp strips at concrete slabs – experiment and modelling. FRPRCS-14 (2019)

[77] fib Task Group 5.1: Externally applied FRP reinforcement for concrete structures

[78] Holzenkämpfer, P.: Ingenieurmodelle des verbundes geklebter bewehrung für betonbauteile. PhD thesis, TU Braunschweig, Germany (1994)

[79] DAfStb: Verstärken von Betonbauteilen mit geklebter Bewehrung: Teil 1: Bemessung und Konstruktion

[80] Finkh, W.: Einfluss bauteilspezifischer effekte auf die bemessung von mit cfk lamellen verstärkten stahlbetonbauteilen. PhD thesis, TU München, Germany (2012)

[81] Niedermeier, R.: Zugkraftdeckung bei klebearmierten bauteilen. PhD thesis, TU

München, Germany (2001)

[82] Rohrer, M., Backhaus, J., Bestmann, U., Arriba López, V., Diaz, P.A., Gerke, M., Könke, C., Lenzen, A., Lippold, L., Maboudi, M., Moeller, M., Villegas, C.L.P., Winkler, P., Zabel, V.: Experimental studies on multi-scale data-driven methods within the framework of structural health monitoring. Civil Engineering Design (2025) https://doi.org/10.1002/cend.202400036

[83] Peeters, B., Roeck, G.: Stochastic system identification for operational modal analysis: A review. Journal of Dynamic Systems, Measurement, and Control **123**(4), 659–667 (2001) https://doi.org/10.1115/1.1410370

[84] Winkler, P., Lippold, L., Zabel, V., Könke, C.: Damage detection combining modal analysis and acoustic emission in concrete structures. Procedia Structural Integrity **64**, 1264–1270 (2024) https://doi.org/10.1016/j.prostr.2024.09.195

[85] Cornwell, P., Doebling, S.W., Farrar, C.R.: Application of the strain energy damage detection method to plate-like structures. Journal of Sound and Vibration **224**(2), 359–374 (1999) https://doi.org/10.1006/jsvi.1999.2163

[86] Stoyan, G., de Boor, C.: A practical guide to splines. applied mathematical sciences 27. berlin-heidelberg-new york, springer-verlag 1978. xxiv, 392 s., dm 32,50. us 17.90. ZAMM - Journal of Applied Mathematics and Mechanics / Zeitschrift für Angewandte Mathematik und Mechanik **60**(1), 62 (1980) https://doi.org/10.1002/zamm.19800600129

[87] Boniface, A., Saliba, J., Sbartaï, Z.M., Ranaivomanana, N., Balayssac, J.-P.: Evaluation of the acoustic emission 3d localisation accuracy for the mechanical damage monitoring in concrete. Engineering Fracture Mechanics **223**, 106742 (2020) https://doi.org/10.1016/j.engfracmech.2019.106742

[88] Kang, C., Walker, M., Marx, S.: Advances of digital twins in bridge structures maintenance. Procedia Structural Integrity **64**, 1232–1239 (2024) https://doi.org/10.1016/j.prostr.2024.09.191

[89] Jansen, A., Herbers, M., Richter, B., Walker, M., Jesse, F., Marx, S.: Monitoring data of the openlab research bridge - part 1: Reference condition. Data in brief **60**, 111624 (2025) https://doi.org/10.1016/j.dib.2025.111624